

Isogeometric Finite Element Modelling of Ideal Non-Linear Free-Surface Flows

Towards total energy conserva-
tion

D.E. Hillege



Isogeometric Finite Element Modelling of Ideal Non-Linear Free-Surface Flows

Towards total energy conservation

by

D.E. Hillege

to obtain the degree of Master of Science
at the Delft University of Technology,
to be defended publicly on t.b.d.

Student:	4384687	
Report:	MT.21/22.027.M	
Thesis Committee:	Jacob Lotz,	TU Delft 3mE, supervisor
	Ido Akkerman,	TU Delft 3mE, supervisor
	Matthias Möller	TU Delft EWI

An electronic version of this thesis is available at <http://repository.tudelft.nl/>.

Preface

Cover image

On this cover image you'll find the author steering the helm of the three masted bark Europa somewhere in the low 40-50 degrees latitude in the Southern Ocean. I remember one night being at the helm in particularly heavy seas in this region. The guests were no longer capable maintaining proper course and we were assigned to helm duty in duo's for good safety measures. My crew mate Lawrence was behind the wheel ensuring we'd keep a proper course. In the mean time I was staring at the large silhouette of ocean chasing the stern of the ship. Each time I saw a really big wave I would think that it was going to break over the ship. Nevertheless, every time this threat posed to be premature as the stern was picked up by this wave and travelled underneath the vessel. All went well up to that unexpected moment when a large dark peak emerged from the night and broke. I shouted at Lawrence to watch out, yet my Dutch accent was not understandable enough to this hardy Irishman in these conditions. I kept repeating myself until Lawrence finally said: "Oh! you mean on your guard." What followed was me and Lawrence, who were luckily attached to safety lines, holding on to each other as the body of water rushed over us. The pressure was high enough for me to open my eyes and see our silhouettes in the water. This thesis further underlined my amazement at how these massive waves seemingly emerge from nowhere. Still, this group of experienced, dedicated and warm hearted people on board this vessel assured my safety as we continued our journey to the Falkland Islands. Although the human race might not follow laws that we designed such that we can coexist in peace, this thesis helped me understand that nature, within the right premise, does follow certain laws. What a comforting thought that we, as a human race, discovered these laws.

Acknowledgements

First and most foremost, I'd personally like to thank all the kindhearted people that are a part of my life and have brought me where I am today. This thesis marks the end of a time which I've both enjoyed and not enjoyed as is with most things in life. As a capstone on top of my education I wanted a challenge which would be a proper scientific endeavour. Naturally, I looked towards Ido and without his vast knowledge of numerical modelling this thesis wouldn't have been possible. The added challenge with working c++ and DelFI was luckily softened with the intensive help of my friend and mentor Jacob without whom this thesis would have taken substantially longer. I'd like to thank both for their support in this thesis and hopefully they will eventually integrate a well documented working numerical towing tank in DelFI. I'd like to thank Ranny for taking the mind of the thesis and having fun on the squash court or climbing gym. My siblings Lize and Wick, who have supported me through all the enduring and challenging times. But most and above all, I'd like to thank my parents, who's unconditional, and sometimes, irrational love has given me the opportunity to seek challenges and succeed or fail.

Summary

Delft University of Technology has access to a towing tank where a wave maker can generate waves. When generating waves, non-linear start-up effects occur at the start of a wave train which affect the rest of the signal. The aim of this thesis is to develop a model which can take these effects into account. A numerical modelling approach is adopted, due to the necessity for generating a large space of wave profiles and the need to optimize towards a wave maker input given a wave profile.

A clear assessment of the state-of-the-art revealed a scope of present methods to model non-linear free surface waves. A potential flow assumption proved a clear balance between accuracy versus computational cost. Analysis of this model showed that the state is described by a balance between potential and kinetic energy and should, in principle, be conserved. For numerical modelling, the Finite Element Method is adopted. The sparse matrices and ease of evaluation of the integrals allow for a better adaptation in present computer architectures. Additionally this method provides more rigorous mathematical tools to demonstrate properties such as stability and convergence. Lastly, the use of Isogeometric Analysis where the solution space is described by splines instead of polynomials could provide an advantage over conventional methods with respect to continuity, convergence and refinement strategies. Subsequently, literature revealed that the potential flow model in conjunction with FEM will result in model that is accurate, stable and fast.

A novel numerical model is presented where the spatial discretization is done using IgA and the resulting semi-discrete Ordinary Differential Equation is integrated in time with a separate method. Analysis shows that this spatial model inhibits the same energy conservation laws as the physical model.

Implementation is done in the DelFI, an in-house fixed domain Navier-Stokes solver with an Open Source back-end named MFEM which utilizes clever FEM abstractions and parallelization. To successfully implement the non-linear problem, first a linear problem is implemented to facilitate computation of variables that are defined on the domain only, in this work the free-surface elevation. This results in introducing an additional problem to compute the elevation on the interior which is dependent on the free-surface, but not vice-versa. This, to ensure the wave problem remains unaffected. Coincidentally, this definition of the free-surface elevation on the interior is used to deform the mesh required to capture non-linear effects in the time-dependent domain.

Results of the linear problem show to agree with literature. Conservation of energy is guaranteed, yet conservation of mass can be attained with sufficient mesh and time resolutions. This affirms the successful implementation of free-surface problems in DelFI. Extension to the non-linear case shows that energy is not conserved, yet analysis shows it should. The same holds for conservation of mass. Still, both quantities can again be contained with sufficient mesh and time resolution. Additionally results demonstrate that implementation of a stabilization scheme is needed. Finally a benchmark case demonstrates that with the current limitations, results agree with others.

This research demonstrated a novel mathematical framework to compute non-linear free surface waves with special emphasis on conservation laws and geometric compliance with the fluid through Isogeometric Analysis. A basis has been laid towards optimization of wave maker signals given a free-surface wave envelope.

Glossary

Acronyms

BEM	Boundary Element Method
CAE	Computer Aided Engineering
CAGD	Computer Aided Geometric Design
CFD	Computational Fluid Dynamics
DOF	Degrees Of Freedom
DUT	Delft University of Technology
FEA	Finite Element Analysis
FEM	Finite Element Method
IgA	Isogeometric Analysis
MOL	Method Of Lines
ODE	Ordinary Differential Equation
PDE	Partial Differential Equation
SUPG	Streamlined Upwind Petrov Galerkin

Greek

α	Coercivity parameter	[-]
η	Free surface elevation	[m]
η_0	Initial free surface elevation	[m]
η_a	Free surface elevation amplitude	[m]
Γ	Boundary	[m ^{d-1}]
γ	Free surface normalisation factor	[-]
κ	Diffusivity parameter	[m ^d /s]
∇	Gradient operator in \mathbb{R}^d	[1/m]
Ω	Domain	[m ^d]
ω	Angular frequency	[rad/s]
ϕ	Solution approximation	[tbd]
ϕ^h	Discrete solution approximation	[tbd]
ψ	Velocity potential	[m ^d /s]
ψ_0	Initial velocity potential	[m ^d /s]
ρ	Density	[kg/m ^d]

θ	Phase	[-]
θ_{wm}	Wave maker angle	[-]
$\tilde{\nabla}$	Gradient operator in \mathbb{R}^{d-1}	[1/m]
Latin		
g	Gravitational vector	[m/s ²]
n	Normal vector	[-]
u	Velocity vector	[m/s]
x	Position vector	[m]
<i>d</i>	Spatial dimension size	[-]
<i>E_{kin}</i>	Kinetic Energy	[J]
<i>E_{pot}</i>	Potential Energy	[J]
<i>g</i>	Gravitational constant	[m/s ²]
<i>H</i>	Wave height	[m]
<i>k</i>	Wave number	[1/m]
<i>L</i>	Wave length	[m]
<i>L_t</i>	Towing tank Length	[m]
<i>p</i>	Pressure	[N/m ²]
<i>R</i>	Source	[tbd]
<i>T</i>	Wave period	[s]
<i>t</i>	Time	[s]
<i>x</i>	x-position	[m]
<i>y</i>	y-position	[m]
<i>z</i>	z-position	[m]

Contents

1	Introduction	1
1.1	Problem definition	2
1.2	Research goal	3
2	State-of-the-art	5
2.1	Gravity free-surface wave theory	5
2.2	Numerical Approximation Techniques	9
2.3	Concluding remarks	14
3	Methodology	15
3.1	Physical Model	15
3.2	Numerical model: space	18
3.3	Numerical model: time	20
3.4	Numerical model: Mesh motion	21
3.5	Arbitrary Lagrangian Eularian (ALE) Frame	22
4	Tools: DelFI & MFEM	23
4.1	Mesh input	24
4.2	Spatial discretization implementation	25
4.3	Output	26
4.4	Flow of control	26
5	Implementation: linear and non-linear wave	29
5.1	Linear wave	29
5.1.1	Version A.	30
5.1.2	Version B.	31
5.2	Non-linear wave	32
6	Results	33
6.1	Linear Wave.	33
6.1.1	Diffusivity dependence	33
6.1.2	Mesh convergence	33
6.1.3	Energy convergence	34
6.1.4	Mass conservation	34
6.1.5	Total potential and free surface	35
6.2	Non-linear wave	36
6.2.1	Energy	38
6.2.2	Mesh convergence	38
6.2.3	Mass conservation	39
6.2.4	Total potential and free surface	39
6.2.5	Comparison of linear free surface with non-linear free surface.	40
6.2.6	Case: Sloshing DNV	41
7	Conclusions & recommendations	43
7.1	Conclusion	43
7.2	Recommendations	44
A	Derivation of Ideal Free-Surface Ideal flow	45
A.1	Bernouilli equations	45
A.2	Boundary condtions	46

B	Mathematical expressions	47
B.1	Reynold's Transport Theorem & Gauss' Divergence Theorem	47
B.2	Definition of kinetic and potential energy.	47
B.3	Green's identities	47
B.4	Boundary integral mapping.	47
B.5	Bilinear form	48
B.6	Luke's Principle	48
C	FEM example: advection diffusion	49
D	Wave maker derivations	51
E	Code Snippets	53
E.1	C++	53
E.2	C	54
F	Running DelFI	55
	Bibliography	57

1

Introduction

High amplitude waves are difficult to predict or simulate at full and model scale. Dysthe et al. [14] states examples where conventional (linear) theories support a very high improbability of large waves occurring at full scale, even though data suggests otherwise. Recently, under prediction of the tsunami resulting from the eruption of the Tongan underwater volcano further underlined the need to keep questioning and improving present models [29]. More accurate prediction methods can give a better understanding of when and why these kind of waves or effects occur and hereby improving on the navigators safety.

Generating waves in ship model tests is important to extrapolate sea-keeping results to field applications. When initiating a wave with a wave maker, undesirable non-linear effects occur at the front of a wave train (Figure 1). These non-linear effects occur in the form of large amplitude waves. Apart from potentially damaging the test setup, it is postulated that these large amplitude waves degrade the rest of the wave envelope.

Currently, linear theory is assumed to arrive at an initial wave profile. After this, the experimentalist still has to tweak the input until a sufficient quality of the wave profile is achieved. Searching such a large domain of possible wave maker inputs by hand is impractical. This lack of data motivates for a numerical modelling approach, allowing for a flexible prediction method of free surface gravity waves. Secondly, it is possible to simulate waves faster than real-time when adopting the right methods. This could be further augmented with automation to converge towards a desired wave envelope.

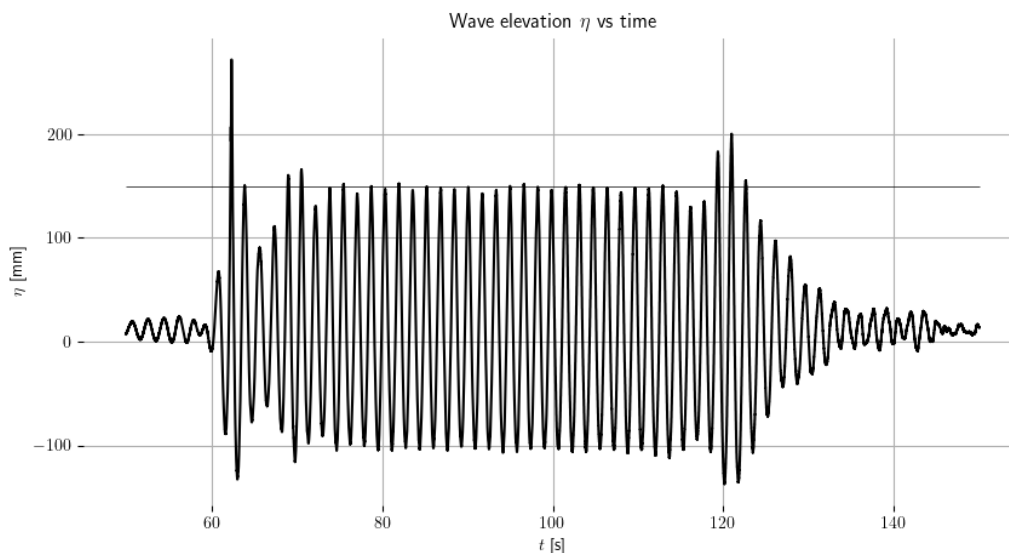


Figure 1: Wave elevation of a probe at DUT at a position x over a time period t . The illustrative black line is plotted to indicate the non constant amplitude from approximately $t = [80, 110]$ (courtesy of Jennifer Rodrigues Monteiro)

1.1. Problem definition

The goal is to improve on current wave predicting techniques. This thesis focusses on the towing tank at the Delft university of technology. This facility hosts towing tank with a wave maker, where model tests can be conducted. Here, the previously mentioned non-linear effects have been observed as well. In Figure 1, a time trace is plotted of the wave elevation at a wave probe. Here, start-up effects of a regular wave can be observed at the start of the time trace. Additionally, the amplitude is non-constant in the interval $t = [80, 110]$. It is postulated that these effects occur due to non-linearity.

The current method at Delft university of technology is to slowly ramp-up the amplitude of the wave-maker (Figure 2). Another method to generate a regular wave, is to use two identical waves as input for the wave maker and slowly matching the phase difference from π to 0 (Figure 3). These methods have not succeeded in solving the problem. An alternative is to develop a digital twin of the towing tank. This digital twin determines the input given the desired wave profile and reduces the start-up effects in the wave train accordingly. This thesis will focus on the numerical modelling of free-surface flows.

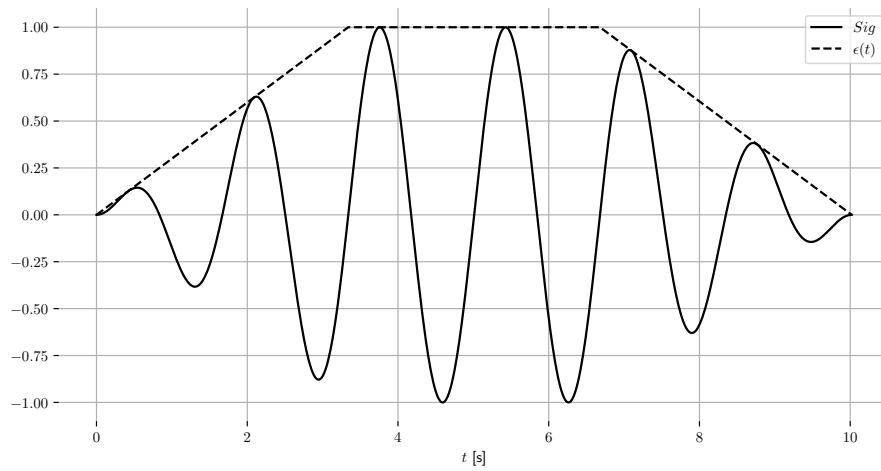


Figure 2: One of the proposed methods where the wave-maker signal is multiplied by a simple ramp up function $\epsilon(t)$.

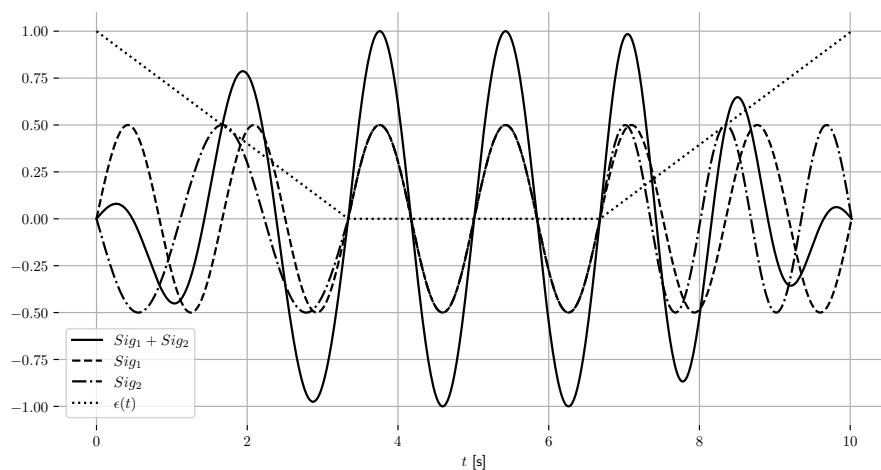


Figure 3: One of the proposed solutions for a wave maker signal. Two signals, where one has a phase shift $\epsilon(t)$. This phase is then linearly decreased to zero resulting in one signal of twice the amplitude of the original signals.

1.2. Research goal

A numerical wave tank consists of a basin, a wave maker and a beach to dissipate the waves. The goal of this research is to numerically model non-linear waves. The underlining requirements are integrated into the main question of this research:

How can we model free-surface waves in an accurate stable and fast way?

Accurate in the sense that the model must closely represent the physical waves. With *stability* we need to ensure that small changes in input will result in small changes in the output. Lastly, the *speed* is required such that the experimentalist improves on the preparation of his/her experiments. The following sub-questions serve to reduce this question into more executable sub-questions.

Chapter 2, *How do we describe waves and their key physical parameters and properties and what techniques can we use to predict them?*

It is important to explore the different methods that have been used to describe and compute free surface waves. From these methods we will converge to a physical model together with a numerical method that fits the main research question accordingly.

Chapter 3, *What are the fundamentals of the selected models and how do these fit the requirements?*

Properties and parameters of the physical model are elaborated after which the numerical method is discussed for linear and non-linear waves. Additionally, properties are derived which serve as a reference to check the computed result.

Chapter 4, *What tools do we need to use in order to model non-linear gravity waves?*

With Computational Science and Engineering as the third pillar of science, thorough understanding of tools that are used in research is important for reproducibility. The platform DelFI in which the numerical model needs to be implemented is discussed.

Chapter 5, *How do we implement our numerical model into DelFI?*

One to one correspondence between abstract analytical representation and the actual model is never evident. Details and challenges will be addressed here. This, in conjunction with the previous question, allows for an individual with knowledge of the topic to be able to reproduce the data.

Chapter 6, *Are the observed results consistent with analysis?*

Here, we will test computation with analysis. Flaws will be easily observed, due to the deductive nature of the chosen method.

Chapter 7, *Which conclusions can we draw from the obtained results and what are the resulting recommendations for future work?*

Lastly, a concluding summary is given outlining critical notes together with recommendations for future work.

2

State-of-the-art

In this chapter we will discuss the Physical flow model in terms of Partial Differential Equations (PDE) and the rationale behind it. Next, a trade-off is made between two dominant numerical approaches for gravity free-surface wave theory. First, the current go-to Boundary Element Method (BEM) is discussed. BEM is then followed by an alternative numerical method, namely the Finite Element Method (FEM) and its potential advantages over BEM. This comparative study will yield an appropriate physical and numerical model for simulating non-linear free-surface gravity waves.

2.1. Gravity free-surface wave theory

In order to implement a suitable numerical model, a physical flow model has to be chosen. For fluids three important properties can be distinguished: conservation of mass, conservation of momentum and conservation of energy. A potential flow can be derived when the fluid is assumed to be inviscid and irrotational [24]. A free-surface is defined when the boundary is free to move. At the free surface a kinematic and dynamic condition are imposed where gravity acts as the stabilizing force ensuring waves can not get too steep. Waves occurring at the free surface stabilized by gravity are called free-surface gravity waves. The potential flow equations augmented with these boundary conditions and initial conditions read: "Given $g \in \mathbb{R}$, $\psi_0 : \Omega(0) \rightarrow \mathbb{R}$ and $\eta_0 : \Gamma(0) \rightarrow \mathbb{R}$, find $\psi : \Omega(t) \rightarrow \mathbb{R}$ and $\eta : \Gamma(t) \rightarrow \mathbb{R}$ such that:"

$$\nabla \cdot \mathbf{u} = \Delta \psi = 0 \quad \text{on } \Omega(t) \text{ (Mass conservation)} \quad (2.1a)$$

$$\psi_{,t} + \overbrace{\frac{1}{2} \|\nabla \psi\|^2}^{\text{Non-linear}} + g\eta = 0 \quad \text{on } \Gamma_{fs}(t) \text{ (Dynamic B.C.)} \quad (2.1b)$$

$$\eta_{,t} + \overbrace{\tilde{\nabla} \psi \nabla \eta}^{\text{Non-linear}} - \psi_{,z} = 0 \quad \text{on } \Gamma_{fs}(t) \text{ (Kinematic B.C.)} \quad (2.1c)$$

$$\nabla \psi \cdot \mathbf{n} = 0 \quad \text{on } \Gamma \setminus \Gamma_{fs}(t). \text{ (No penetration B.C.)} \quad (2.1d)$$

Here g is the gravitational constant, \mathbf{n} the outward pointing normal, ψ the potential and η is the free surface elevation. $\tilde{\nabla}$ is the two dimensional gradient operator. Note that mass conservation (A.17) is equivalent to the Laplace equation.

Analytical modelling of free surface flow One could adopt an analytical model for free-surface waves where the potential and free-surface elevation are explicitly defined and hereby omitting the need of computational methods. However, analytic descriptions of waves have only been found for simple cases. We will illustrate two examples by the Airy wave and second order Stokes wave. For the Airy wave, the non-linear terms in the boundary conditions at the free surface are disregarded. This is the case when waves are assumed not to be too steep due to a small wave number k ($\eta_a k \ll 2\pi$). This is also the case when the amplitude η_a is sufficiently small with respect to the water depth d ($\eta_a \ll d$). The solution for the free surface elevation and

potential are [20]

$$\eta(x, t) = \eta_a \sin(\omega t - kx) \quad (2.2)$$

$$\psi = \frac{\omega \eta_a}{k} \frac{\cosh(k(d+z))}{\sinh(kd)} \cos(\omega t - kx). \quad (2.3)$$

The angular frequency ω and wave number k are related through the linear dispersion relation

$$\omega^2 = kg \tanh(kd). \quad (2.4)$$

For Stokes waves, the momentum balance (See Appendix (A.16)) is expanded at the free surface level $y = \eta$ to the undisturbed free-surface $y = 0$. The momentum balance is given independent from the free surface elevation if the material derivative for the pressure is taken to be zero [36]

$$\frac{Dp}{Dt} = \left(\frac{\partial}{\partial t} + \nabla \phi \cdot \nabla \right) \left(\frac{\partial \phi}{\partial t} + \frac{1}{2} \nabla \phi \cdot \nabla \phi + gy \right) = 0. \quad (2.5)$$

From this expression the potential is derived up to a desired order. The free surface elevation is derived by substituting this potential into the momentum balance which is explicitly dependent on the free surface elevation. The solution (plotted in Figure 4) for second order Stokes potential and wave elevation are

$$\psi = \psi^{(1)} + \psi^{(2)} = \frac{\omega \eta_a}{k} \frac{\cosh(k(d+z))}{\sinh(kd)} \sin(\omega t - kx) + \frac{3\omega \eta_a^2}{k} \frac{\cosh(2k(d+z))}{8 \sinh^4(kd)} \sin(2\omega t - 2kx) \quad (2.6)$$

$$\eta = \eta^{(1)} + \eta^{(2)} = \eta_a \cos(\omega t - kx) + k \eta_a^2 \frac{\cosh(kd)(\cosh(2kd) + 2)}{4 \sinh^3(kd)} \cos(2\omega t - 2kx). \quad (2.7)$$

These equations are subject to the first order dispersion relation given in Equation (2.4).

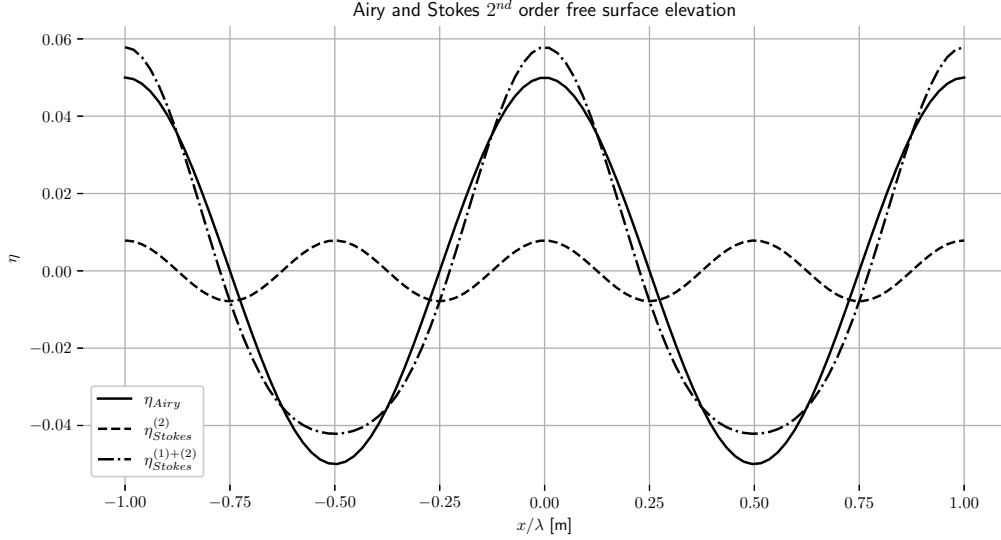


Figure 4: Plot of analytical solutions of linear Airy and non-linear Stokes waves for a depth $d = 1$, wavelength $\lambda = 1$ and amplitude $\eta_a = 0.05$. Note the flatter troughs and sharper peaks for the Stokes waves

These analytical expressions provide valuable understanding of free surface gravity waves and its key parameters, but are limiting with respect to applicability (see Figure 5). Secondly, these cases are often restricted to steady problems.

The goal is to be able to model a wide range of wave envelopes. From variable depth to substantial steepness within the bounds of the potential flow assumption. Additionally, there is a need to model unsteady behaviour as well as an irregular envelope to study non-linear wave-wave interaction. Current explicit analytical descriptions offer a tool to understand fundamental physical properties, yet lack a description conforming to reality. Numerical modelling provides a method where such flexibility is guaranteed.

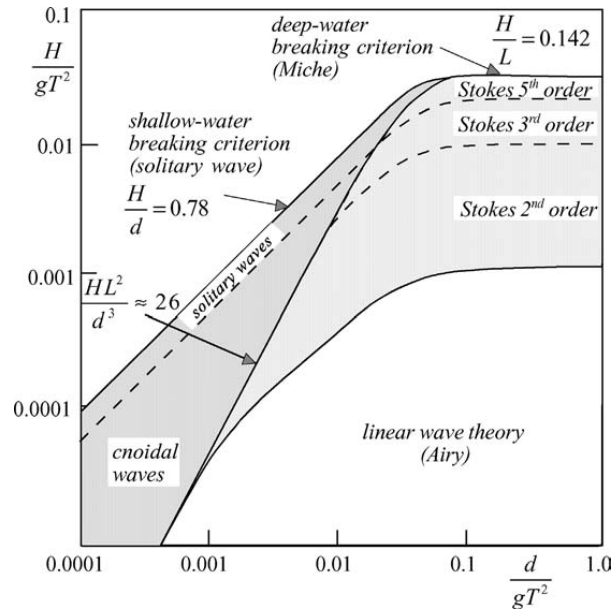


Figure 5: Applicability of different wave theories [20]. The index HL^2/d^3 is an indication of the wave steepness over the (relative depth)³. Also referred to as the Ursell number. Here, H is the wave height, L is the wavelength and $T = 2\pi/\omega$ is the wave period.

Computational modelling of free surface flow Apart from using analytical expressions, a more general approach is to take a set of PDE's describing the physics with appropriate boundary conditions. The next step is to adopt a numerical method to approximate the derivatives and solve for the unknown potential and free-surface height. Herein, a choice can be made to solve the full non-linear governing equations or an approximated/reduced form of the governing PDE's under the premise that some property, e.g. wavelength or steepness, is dominant over others [8][41]. The shallow water Boussinesq equations are such a reduced form. These approximated cases have the advantage that when used in conjunction with numerical methods provide cost efficient models to predict a wave. These cases are divided into two classes. When the amplitude η_a is much larger than the wave number k (i.e. $\eta_a k \ll 1$) the solution is in the shallow water regime. These shallow water waves are also called steep waves. The second class is the deep water limit. Here the amplitude should be much smaller than the water depth d for deep water, i.e. $\eta_a \ll d$ [20].

A requirement for model tests in towing tanks is the possibility of generating waves at a wide range of wavelengths and finite depths. Secondly, Figure 1 indicates that different waves do interact with each other non-linearly. This is due to the fact multiple frequencies are observed in the signal, even though the source is harmonic. The incompressible Navier-Stokes equations are physically the most accurate for water-flow. Still, a potential flow model shows to be sufficiently accurate for non-linear free-surface gravity waves up to a certain wave steepness or water depth. This reduces the computational costs considerably.

In Brink et al. [7], non-linear potential flow theory is used to predict deep water rogue waves. In Gidel [17] this is further extended to predict deep water waves and coupled to a finite volume method to compute shallow water waves which can break. In both studies, validation is done by generating a wave and measuring the output. The movement of the wave maker is recorded as well. The wave maker motion is then used as input for the model. The methods presented in both papers shows to have good agreement with reality. This justifies the use of a potential flow model.

In order to successfully implement these equations into a discretized form one can make use of conservation laws from which the PDE is derived. From this scalar conservation function a minimization problem can be derived. Consequently, a solution of the minimization problem, means a solution of the PDE. Here, we could make use of the conservation of energy that is inherent to ideal flow [37].

Energy properties of potential flow Potential flow is also referred to as an ideal flow. This is due to the energy state of the fluid. The fluid is ideal in the sense that no energy loss occurs through viscous or vortex dissipation [35]. With Kelvin's circulation theorem this can be shown. What remains is only the Kinetic energy E_{kin} and the Potential energy E_{pot} . Two energy statements for the kinetic and potential energy are

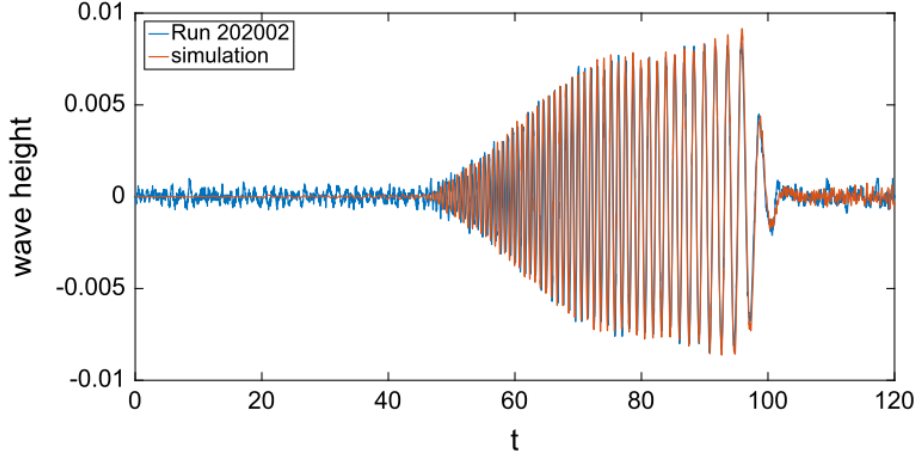


Figure 6: Match between potential flow model from [7] and experimental data provided by MARIN.

distinguished in the field of classical mechanics [35].

$$L = E_{kin} - E_{pot} \quad (2.8)$$

is the Lagrangian description, with L being the Lagrangian. The Hamiltonian description H is given by

$$H = E_{kin} + E_{pot} \quad (2.9)$$

These descriptions are related when we consider the variation δL and δH of L and H [5][35]. This time conservation statement is of special importance for numerically solving wave problems, due to its physical relevance regarding phase and amplitude errors.

To illustrate this, for a regular numerical wave with a phase θ^h we can define an amplification factor $\lambda = 1 + \epsilon$ by which θ^h is amplified due to an error ϵ . For a time step n , which is denoted by the superscript, we have

$$\theta_1^h = \lambda \theta_0^h \quad (2.10)$$

$$\theta_2^h = \lambda \theta_1^h \quad (2.11)$$

$$\vdots \quad (2.12)$$

$$\theta_n^h = \lambda \theta_{n-1}^h. \quad (2.13)$$

Through induction one can derive $\theta_n^h = \lambda^n \theta_0^h$. The desired requirement from an energy conservation point of view is $|\lambda| = 1$. When this factor is not equal to unity the global error increases or decreases with each time step. Additionally, any error made at an instance remains in the solution and can negatively affect the solution, due to the absence of damping or dissipation. Accordingly, it is important for a numerical method that physical properties are carried over into the numerics and sufficient accuracy is maintained.

Methods that adopt the energy conservative properties of potential flow are demonstrated in [7] and [17]. Their energy expression is referred to as a Hamiltonian structure. A Hamiltonian structure is a variational statement in which the motions of a Newtonian potential system coincide with the extrema of this statement [5][8]. Physically, a certain quantity is minimized with respect to some physical parameters. This is equivalent to stating that a particle seeks the path of minimal resistance. Examples are the brachistochrone or the hanging cable problem. For the case of the non-linear gravity wave problem in [7] and [17], a variational statement was derived by Luke [28]. Here, the pressure is postulated to be the conserved quantity.

In Luke's variational principle the physical parameters are the free-surface height η and potential ψ . These parameters are constrained to $\delta\eta(x_1, x_2, t_1, t_2) = 0$ and $\delta\psi(x_1, x_2, t_1, t_2) = 0$ to satisfy a solution. Luke's statement minimizes the following functional:

$$J = \int_{t_0}^{t_1} \int_{x_0}^{x_1} \mathcal{L} dx dt$$

, with

$$\mathcal{L} = \int_0^{\eta(x,t)} (p - p_0) d\Omega = - \int_0^{\eta(x,t)} \left(\frac{1}{2} \psi_x^2 + \frac{1}{2} \psi_y^2 + \psi_{,t} + g(y - H_0) \right) dy$$

begin the variation of the pressure. If we vary the functional J accordingly with respect to η and ψ at the boundaries, Luke states the following:

$$\delta J = \int_{t_0}^{t_1} \int_{x_0}^{x_1} \delta \mathcal{L} dx dt = 0$$

To arrive at.

$$\begin{aligned} \delta \mathcal{L} &= \left[\frac{1}{2} \|\nabla \psi\|^2 + \psi_{,t} + g(y - H_0) \right]_{y=h} + \int_0^{\eta(x,t)} \nabla \psi \cdot \nabla (\delta \psi) + \delta \psi_{,t} dy \\ \Rightarrow \delta J &= \int_{t_0}^{t_1} \int_{x_0}^{x_1} \left\{ \left[\frac{1}{2} \|\nabla \psi\|^2 + \psi_{,t} + g(y - H_0) \right]_{y=h} \delta \eta + \int_0^{\eta(x,t)} \nabla \psi \cdot \nabla (\delta \psi) + \delta \psi_{,t} dy \right\} dx dt = 0 \end{aligned} \quad (2.14)$$

For an expanded derivation see Appendix B. From this functional the correct potential flow equations are obtained for the interior and boundaries after integration by parts and by first setting $\delta \eta = 0$ and allowing for ψ to vary and then $\delta \psi = 0$ and allowing η to vary. As such, the variational formulation shows to be consistent with the governing equations.

$$\begin{aligned} \frac{1}{2} \psi_{,x}^2 + \frac{1}{2} \psi_{,y}^2 + \psi_{,t} + g(y - H_0) &= 0 && \text{at } \Gamma_{fs}(t) \\ -\eta_{,x} \psi_{,x} + \psi_{,y} - \eta_{,t} &= 0 && \text{at } \Gamma_{fs}(t) \\ \psi_{,y} &= 0 && \text{at } y = 0 \\ \psi_{,xx} + \psi_{,yy} &= 0 && \text{on } \Omega(t) \end{aligned}$$

A property of the variational statement, is that it provides a single scalar expression for both the interior as well as the boundary in which energy is conserved due to $\delta J = 0$.

In this case the variational formulation starts from an energy principle which is conserved. This means that the problem is a minimization problem and suitable for discretization with the finite element method. In [7] this method is used a priori to derive a conservative numerical model. In [1] & [2], energy conservation is derived a posteriori.

2.2. Numerical Approximation Techniques

Numerical modelling of non-linear waves consist of solving continuous (partial) differential equations through discretization. To numerically solve the strong form of the potential flow equations, two approaches are mainly present in literature. One is to use BEM [10][11][32][38] and the other is to use FEM [2][7][17][23].

Boundary Element Method

BEM is a well established method in the maritime industry [10][26][32][38]. With these methods, the application of Green's second identity on the interior effectively reduces the dimension of the problem by one. A result of this is that the entire fluid potential is described only by its boundaries [6] or a so-called boundary integral equation. The integral for $\psi : \Omega(t) \rightarrow \mathbb{R}$ is given by

$$4\pi T \psi(\vec{x}) = \int \int \left[\frac{\partial \psi}{\partial n_\xi}(\vec{\xi}) G(\vec{\xi}, \vec{x}) - \psi(\vec{\xi}) \frac{\partial G}{\partial n_\xi}(\vec{\xi}, \vec{x}) \right] dS_\xi \quad (2.15)$$

with ψ the velocity potential, T is a variable dependent on the position. This can be inside the domain, on the boundary or outside of the domain. The normal pointing into the fluid is n_ξ , ξ is the position with respect to the potential source, G is a Green's kernel function, and dS_ξ the bounding surface.

Solution methods present itself by solving the integral using a Galerkin approximation or using the linear properties of the Laplace equation (A.17) on the full fluid domain.

Galerkin BEM The Galerkin method [15] is a weighted residual method [44]. A weighted residual method is a method where the continuous integral is multiplied by a weighting function, which is part of the solution, and integrated over. The residual states that this integral has to be minimized, i.e. equate to zero. This continuous statement is then split into a discrete subset such that the potential can be approximated as the sum of these discrete elements suitable for linear computation.

The integrals form a dense system. This dense system poses additional computational challenges and requires different solvers than the traditional $O(N^2)$ solvers with N unknowns [13][15]. For example, solving these systems can be done using Fast Fourier Transforms [15] or Fast Multipole methods [13]. Additionally, due to the Green's function, a singular integral has to be evaluated. As a result, appropriate techniques in conjunction with standard quadrature rules have to be used [18][31].

The advantage of using Galerkin BEM over collocation methods discussed in the next section, is that the method gives more control regarding smoothness over the entire geometry. In contrary to collocation methods where boundary conditions only have to be met pointwise in collocation points. With Galerkin BEM the solution is defined by the weighting function, which is continuous up to a certain order. For instance, one could opt for a second order polynomial. This imposes C^2 continuity across the elements. Similar conditions can be imposed between elements. This enhanced control over the solution allows for more thorough analysis of the method over collocation methods at the cost of complexity.

For the case of free boundaries, such as a free surface, studies were not found. In retrospect, these types of problems are mainly presented with an emphasis on techniques which allow for efficient solving of dense matrix vector equations and singular integrals. Applied physical problem solving do not seem to be the main criteria, limiting this method to academia only.

Collocation methods The use of sources and sinks is a method which is widely adopted in Maritime applications [10] [19] [25] [32] [38]. Due to the harmonic Laplace equation for the interior, the velocity potential is described by a sum of harmonic functions, namely sources and sinks over the boundaries [32] [38]. The sum of these functions approximates the global flow. For a moving body or surface, the contribution of a singularity ϕ_i in its collocation point has to relate to that of the singularities $\phi_{j \neq i}$ such that the boundary conditions are met, whereas for Galerkin BEM this has to be satisfied over the entire boundary. Accordingly, a dense system of equations is derived that solves for the flow.

Raven [32] developed a code for the non-linear steady problem called RAPID (RAised Panel Iterative Dawson). Here, panels are used as singular potential valued sources and sinks. This method has been used extensively to predict the wave-making resistance of ships and has proven its capabilities.

RAPID solves the potential flow equations by assuming an initial free surface η and velocity potential distribution ϕ and iteratively solve for the kinematic and dynamic boundary conditions. The main distinction from other methods is that the panels corresponding with the free surface are in this case raised above the free surface. The collocation points remain on the free surface.

For the free surface a linearised perturbation is assumed for the velocity and elevation. The dynamic boundary condition can then be substituted in the kinematic boundary condition. Although Raven [32] shows that the raised panels are superior over placing the panels at the free surface, energy loss occurs when evaluating the derivatives at the free-surface.

Secondly, Raven [32] shows that numerical dispersion is apparent for his improved scheme. For a steady problem such as RAPID this might not pose as much as a problem as for an unsteady problem where numerical dispersion results in phase errors with each time step.

Lastly, the author gives considerable doubts regarding the robustness of the method [32]. In addition, these observations were in line with other work [11][38]. Sclavounos [34] does give some indications on consistency and stability, but are nearly not as rigorous as the derivations presented in Finite Element Methods, such as Galerkin BEM.

Boundary Integral Methods provide an attractive solution method for solving a scalar potential equation, due to reduced dimensionality as a result of the Green's function. This reduced number of unknowns to solve for does, however, come with dense matrices and additional solution techniques to evaluate singular integrals for the case of Galerkin BEM. The less strict/formal approach in collocation methods shows to be an easier adaption for industry purposes. However, unintended diffusion is introduced when evaluating derivatives at the free-surface and to make the system solvable relaxation factors have to be introduced. An extension of the method of weighted residuals called FEM could provide an alternative. Now applied on the full domain, this method is mathematically more challenging, but allows firm analysis if needed.

Finite Element Analysis

FEM is a widely adopted method for approximating partial differential equations [22][40]. The resulting system of equations that needs to be solved is larger, as the entire volume needs to be discretized. In contrast, FEM is locally coupled, also known as compact support, which results in solving sparse systems. These sparse systems are then again suitable for implementation of parallel computation methods. Literature on linear and non-linear potential flow for Finite Elements is rather extensive [2][7][17][23][39][43]. Here, a clear distinction is observed between a decoupled [23][43] and a monolithic formulation [2][7][17][39]. With decoupled we mean separate or implicit treatment of the boundary and interior problems.

Energy non-conserving methods In [23] and [43], first the interior problem is solved for the velocity potential. From the interior problem, the velocity potential values on the free surface are used to evolve the free-surface solution in the time domain. Hereafter, the interior problem is solved and the process starts over again. This approach decouples the boundary problem from the interior problem, whilst they are physically connected.

Westhuis [39] recovers the velocity from the gradient of the potential. The grid is adjusted by means of this velocity and the kinematic and dynamic boundary conditions are solved for. Although this method might seem of an intuitive approach, an order of continuity for the velocity is lost due to derivation of the shape function. Secondly, this approach still serves as a multistep method and hereby not solving the complete problem in a coupled or monolithic fashion.

In effect, for both approaches an explicit energy statement is no longer present, even though energy conservation is guaranteed in the strong form of the problem. Ideally, these properties are present in the numerical scheme as well. Results from Kim and Bai [23] and Wu and Eatock Taylor [43] lead to small, but present phase errors. This can pose problems when dealing with unsteady non-linear problems. A mathematical tool that combines the boundary problem and the interior problem into one expression are so-called variational principles.

Energy conserving methods In Brink et al. [7] the functional from Luke [28] is discretized after which the variations are taken to obtain the discrete variational principle. Gidel [17] does the opposite. Here, the variational principle is derived after which the weak form is derived. The discrete variational principles are written in Hamiltonian form to arrive at an energy conservation statement. Both methods show to lead to good energy conservation behaviour.

In Akkerman et al. [2], an energy statement is shown as the time evolution of the sum of the potential and the kinetic energy. This method is reduced to the linearised case, but computed using the novel methodology of Isogeometric Analysis (IgA). They also show boundedness and accuracy of the solution. The results presented in this paper show some good properties of using Non-Uniform Rational B-Splines (NURBS) over conventional basis functions regarding (phase) accuracy and convergence (Figure 25) as well as smoothness. The number of elements required also shows to be much less than in conventional FEM [7][17][39].

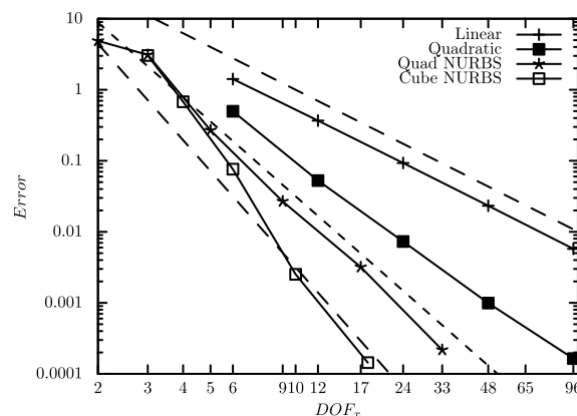


Figure 7: h-refinement convergence of the method presented in Akkerman et al. [2] compared to linear and quadratic FE

Isogeometric Analysis

Isogeometric Analysis (IgA) is a framework introduced in Hughes et al. [21]. This method aims to close the gap between Computer Aided Geometric Design (CAGD) and Computer Aided Engineering (CAE). Geometry within CAGD is defined by means of parametric splines, whereas in CAE a different geometric description is used¹. This discrepancy results in a geometric error when performing analysis. Due to the much larger market capitalization of CAGD, [21] asserted that the branch of CAE should conform to that of CAGD. Apart from the computational benefit, labour costs are also partly reduced now that less time is involved in transferring the CAGD spline mesh to a CAE mesh.

Isogeometric analysis diminishes the geometric error between GAGD and CAE. Often, the solution space of dependent variables is in a different mathematical description than that of the design. Meshing processes involve transferring the geometry description to one that is suitable for analysis. Hughes et al. [21] aims to omit this step by describing the solution mesh in the same function space as the geometry.

Hughes et al. [21] describes NURBS based Isogeometric Analysis. Here the geometric *and* solution space is described by NURBS. However, different methods of describing geometries are also optional [33][30]. A B-spline *basis function* is recursively defined through

$$N_{i,p}(\xi) = \frac{\xi - \xi_i}{\xi_{i+p} - \xi_i} N_{i,p-1}(\xi) + \frac{\xi_{i+p+1} - \xi}{\xi_{i+p+1} - \xi_{i+1}} N_{i+1,p-1}(\xi) \quad (2.16)$$

Here, p is the order and i is the index of the knot vector Θ having value ξ_i . In other words $\xi_i \in \Theta$. The zeroth and first order splines are equivalent to their polynomial counterparts. For second and higher order splines, this similarity disappears (see Figure 8). A B-spline *curve* $C(\xi) \in \mathbb{R}^d$ is defined by a linear combination of basis

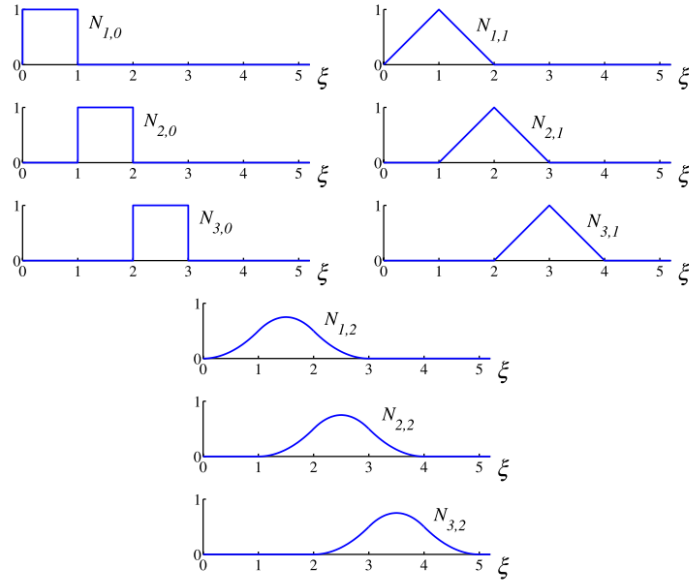


Figure 8: NURBS based basis functions of order 0, 1, 2 for uniform knot vector $\Theta = \{0, 1, 2, 3, 4, \dots\}$.
From [21]

functions

$$C(\xi) = \sum_{i=1}^n N_{i,p}(\xi) B_i \quad (2.17)$$

Here, $B_i \in \mathbb{R}^d$ is a corresponding control point and d the dimension of the Cartesian space.

Some key advantages of NURBS based IgA adopted from [21] are:

1. Exact design geometry (also through refinement)
2. k-refinement

¹e.g. polynomials or wavelets

3. Total variation diminishing property (TVD) of NURBS

Exact geometry is retained through refinement with knot insertion. In this process, the exact geometry is retained of the original curves. Retaining the same geometry through refinement is ideal, albeit not always guaranteed in conventional FEM.

Another refinement strategy called k-refinement presented by [21] allows for a refinement and order elevation strategy where no loss of continuity occurs within the original element. For an element of order h , C^{h-1} -continuity is maintained through the refinement process. With conventional FEM, if n extra elements are added due to refinement, then also n nodes over which C^{h-1} continuity occurs are added. Consequently, both refinement strategies (knot insertion and k-refinement) show to be superior of that over conventional basis functions.

The TVD property shows to be effective near sharp changes in the solution, e.g. boundary layers. When fitting discontinuous data, a conventional Lagrange interpolation shows spurious results when elevating order. With NURBS this behaviour is not observed for the same data. In [21] this is illustrated by an example of skewed advection with outflow Dirichlet boundary conditions.

Akkerman et al. [2] presented a linearised case for a free-boundary problem regarding potential flow. They showed that a linear wave can accurately be described by only four DOF's [2], whereas for other methods this is generally higher [32] [7] [17]. Momentum can be approximated with less DOF's using present methods. Secondly, IgA shows to have superior convergence properties over conventional basis functions. The method presented in [2] also shows energy correct behaviour of the method allowing for long time duration simulations in wave problems.

2.3. Concluding remarks

The state-of-the-art is assessed in non-linear water wave analysis. The framework needed for a digital twin wave-maker consists of a flow description, solution methods and optimization techniques. In summary, a succinct list of the conclusions drawn from this chapter is:

- A potential flow description provides a fast and reliable alternative for non-linear water waves over viscous models. Requirements for a numerical scheme are phase and amplitude accuracy together with energy conservation.
- The reduced number of unknowns that come with a boundary element method is not necessarily advantageous over the Finite Element method where compact support results in sparse matrices.
- Additionally, the Finite Element allows for a more robust, accurate and precise method over the Boundary Element Method.
- The use of NURBS in FEM can lead to coarser meshes, yet retaining accuracy and reducing computational cost.

A comparison of the key literature and the proposed method is listed in Table 1

Table 1: Properties of different methods presented in literature. The different properties are Linear Potential Flow(LPF), Non-Linear Potential Flow(NLPF), Boundary Element Method (BEM), Finite Element Method and Isogeometric Analysis (IgA).

	$dE/dt = 0$	$\partial/\partial t \neq 0$	LPF	NLPF	BEM	FEM	IgA
van Walree [38]		x	x		x		
Raven [32]				x	x		
Brink et al. [7]	x	x		x		x	
Gidel [17]		x		x		x	
Akkerman et al. [2]	x	x	x			x	x
Proposed method	x	x		x		x	x

3

Methodology

In this chapter methods are discussed that describe the physics which again can be computed using numerics. The physical model distinguishes from the numerical model in the sense that a physical model serves as a mathematical model to describe the relation between physical variables by means of partial differential equations. These PDE's are augmented by boundary conditions in order to complete the problem description. A system of PDE's and its boundary conditions can then be approximated using a numerical method. The numerical method aims to approximate these variables, such that the PDE's and its boundary conditions are valid at a given time and place up to a certain accuracy.

3.1. Physical Model

Physical modelling involves deriving mathematical descriptions for physical processes. Similarly, many well known mathematical equations can be linked to physical processes. Examples are the heat equation or the advection diffusion equation. Physical models are generally derived from a conservation principle, e.g. conservation of heat, mass, momentum or energy. For fluid flow we can imply conservation of momentum[24]. This, added with conservation of mass and the requirement that the fluid does not change density, yields the incompressible Navier-Stokes equations, where *given* the density $\rho \in \mathbb{R}$, gravitational vector $\mathbf{g} \in \mathbb{R}^d$ and kinematic viscosity $\mu \in \mathbb{R}$, we aim to *find* the velocity $\mathbf{u} : \Omega(t) \rightarrow \mathbb{R}^d$ and pressure $p : \Omega(t) \rightarrow \mathbb{R}^d$, such that

$$\rho \mathbf{u}_{,t} + \rho(\mathbf{u} \cdot \nabla) \mathbf{u} = -\nabla p + \rho \mathbf{g} + \mu \nabla^2 \mathbf{u} \quad (3.1a)$$

$$\nabla \cdot \mathbf{u} = 0. \quad (3.1b)$$

Assumptions

The Navier-Stokes can be non-dimensionalized (see Appendix A). Properly selecting the physical parameters for the pressure and non-dimensionalizing displays the relevant non-dimensional numbers. For non-breaking free-surface water waves in the inertial regime we can make the following assumptions [7][17].

1. Incompressible on Ω
2. Irrotational on Ω
3. No surface tension on Γ_{fs}
4. No overturning waves on Γ_{fs}

Under these assumptions the Navier-Stokes equations reduce to a potential flow formulation. The resulting fluid description is also referred to as a perfect or ideal fluid. The fluid is perfect in the sense that the net energy change can only be a result of the boundary conditions. This can be shown through Kelvin's circulation theorem.

Governing equations

The governing equations for free-surface potential flow are recited: *given* the gravitational constant $g \in \mathbb{R}$ we aim to *find* the potential $\psi : \Omega(t) \rightarrow \mathbb{R}$ and free-surface elevation $\eta : \Gamma_{fs}(t) \rightarrow \mathbb{R}$ such that

$$\Delta\psi = 0 \quad \text{on } \Omega(t) \text{ (Mass conservation)} \quad (3.2a)$$

$$\psi_{,t} + \overbrace{\frac{1}{2} \|\nabla\psi\|^2}^{\text{Non-linear}} + g\eta = 0 \quad \text{on } \Gamma_{fs}(t) \text{ (Dynamic B.C.)} \quad (3.2b)$$

$$\eta_{,t} + \overbrace{\nabla\psi \nabla\eta}^{\text{Non-linear}} - \psi_{,z} = 0 \quad \text{on } \Gamma_{fs}(t) \text{ (Kinematic B.C.)} \quad (3.2c)$$

$$\nabla\psi \cdot \mathbf{n} = 0 \quad \text{on } \Gamma \setminus \Gamma_{fs}(t). \text{ (No penetration B.C.)} \quad (3.2d)$$

The non-linear terms are annotated in the governing equations (3.2). When the wave is assumed to be linear, these terms are dropped. The linear boundary conditions with the Laplace equation 3.2a imply that any linear wave can be described as the sum of individual linear components. This simplifies solution methods and implementation considerably. When the non-linear terms are not disregarded this is no longer valid.

$$\eta(x, t) = \sum_{i=0}^n a_i \sin(k_i x - \omega_i t + \theta_i) \quad \text{Linear assumption}$$

$$\eta(x, t) \neq \sum_{i=0}^n a_i \sin(k_i x - \omega_i t + \theta_i) \quad \text{Non-linear}$$

Boundary and initial conditions

The governing equations can be augmented by boundary conditions and initial conditions resulting in a description suited for computation.

$$\nabla\psi \cdot \mathbf{n} = 0 \quad \text{on } \Gamma \setminus (\Gamma_{fs} \cup \Gamma_R) \quad (3.3a)$$

$$\nabla\psi \cdot \mathbf{n} - \dot{S} = 0 \quad \text{on } \Gamma_R. \quad (3.3b)$$

$$\psi(\mathbf{x}, t = 0) = \psi_0 \quad \text{on } \Omega \text{ (Initial condition)} \quad (3.3c)$$

$$\eta(\mathbf{s}, t = 0) = \eta_0 \quad \text{on } \Omega \text{ (Initial condition)} \quad (3.3d)$$

Equation (3.3a) refers to as a no-penetration condition, implying no fluid can travel through this boundary. A moving boundary can be described with equation (3.3b) where $S : \Gamma(t) \rightarrow \mathbb{R}$, describes the moving boundary, which is not a part of this thesis. One of the initial conditions (3.3d) or (3.3c) can be imposed if the solution for either the potential or free-surface at $t = 0$ is known. For a sloshing case, this could be an initial perturbation of the free-surface.

Geometric parameters for the free surface

For the free surface, additional parameters can be derived which are of use to prove properties a of numerical method for the non-linear case. Additionally, they can be substituted to follow boundary conditions. Irrotationality implies that the velocity field derives from a potential

$$\mathbf{u} = \nabla\psi$$

The free surface $\eta(x, y, t)$ equation is defined to be the level-set

$$z - \eta = 0.$$

The normal on the free-surface is defined as

$$\begin{aligned} \mathbf{n} &= \frac{\nabla(z - \eta)}{\|\nabla(z - \eta)\|} \\ &= \frac{1}{\sqrt{1 + \|\nabla\eta\|^2}} \begin{bmatrix} -\nabla\eta \\ 1 \end{bmatrix} \end{aligned}$$

We can derive some equalities on the free surface by using this expression where we take the dot product of the normal with the velocity potential and substituting the kinematic boundary condition.

$$\begin{aligned}
 \gamma &= \frac{1}{\sqrt{1 + \|\nabla\eta\|^2}} \\
 \nabla\psi \cdot \mathbf{n} &= \gamma \begin{bmatrix} -\nabla\eta \\ 1 \end{bmatrix} \nabla\psi \\
 &= \gamma(\psi_z - \nabla\eta \nabla\psi) \\
 &= \gamma\eta_t \\
 \Rightarrow \nabla\psi \cdot \mathbf{n} &= \mathbf{u} \cdot \mathbf{n} = \gamma\eta_{,t}
 \end{aligned} \tag{3.4}$$

Problem setup

The problem setup describes the parameters and geometrical description of the domain. For a numerical towing tank the body of water is initially at rest after which the wave maker starts to move. In this thesis we will restrict the domain without a wave maker. The aim is to replicate the linear wave from Akkerman et al. [2] in DelFI first. When this is achieved, the non-linear case extension to Akkerman et al. [2] is implemented.

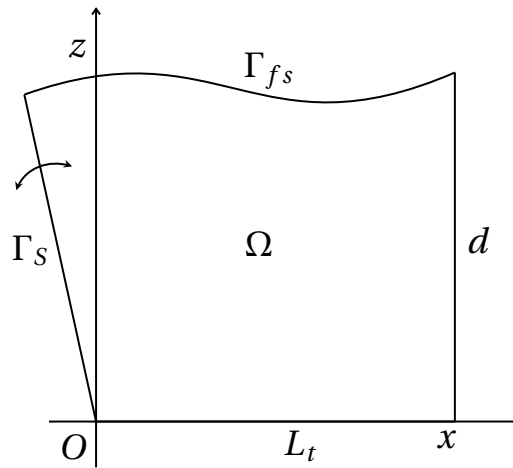


Figure 9: Schematic representation of the problem setup of a numerical towing tank. L_t denotes the length of the towing tank and d denotes the water depth.

3.2. Numerical model: space

Numerical modelling is a technique where the continuous physical model is approximated using a numerical method. The PDE's are discretized with a method of choice such that the physical model is followed as closely as possible at any state. Discretization is the partitioning of the continuous domain into a set of discrete points or domains. For a time dependent problem this has to be done both in space and time.

Spatial discretization is done using the Finite Element Method resulting in a semi-discrete system of equations. With the Finite Element Method, the solution functions are approximated by weighing them by test functions. In practice this involves multiplying the *trial/solution* function space by a *test* function space and integrating over, resulting in a weak form. Green's identities (B.5) can be used to reduce the order of the PDE, with which boundary terms arise. Boundary conditions that can be substituted implicitly from Green's identities are called *natural boundary conditions*. Boundary conditions that have to be defined explicitly are called *essential boundary conditions*. Discretization stems from the partition of the domain of this weak form into a discrete subset and describing the solution in each subdomain by means of a simple function times a weight. The Linear combination of these basis functions approximates the integral defined by the weak form.

Linear wave

For the linear wave we first start with the strong form of the problem and work towards the weak or variational form.

Strong form The strong form of the linear problem reads:

$$\begin{aligned} \Delta\psi &= 0 && \text{on } \Omega \text{ (Mass conservation)} \\ \psi_{,t} + g\eta &= 0 && \text{on } \Gamma_{fs} \text{ (dynamic B.C.)} \\ \eta_{,t} - \psi_{,z} &= 0 && \text{on } \Gamma_{fs} \text{ (kinematic B.C.)} \\ \nabla\psi \cdot \mathbf{n} &= 0 && \text{on } \Gamma \setminus \Gamma_{fs} \end{aligned}$$

Weak form The strong form is multiplied by their respective test functions and integrated over the domain. The interior term can be reduced with integration by parts and Gauss' divergence theorem. The identities in equation (3.4) are used to substitute the kinematic boundary condition. For the linear case, γ is equal to one. Clearly, if $\gamma = 1$, then the boundary term is only a function of the undisturbed free-surface. The dynamic boundary condition relates ψ to η only in time and can also be computed with respect to the undisturbed free-surface. With the notation

$$\begin{aligned} (b, c)_{\Omega} &= \int_{\Omega} ab \, d\Omega \\ (b, c)_{\Omega} &= \int_{\Omega} \mathbf{a} \cdot \mathbf{b} \, d\Omega \end{aligned}$$

The weak form formulates to

$$\begin{aligned} -(w, \Delta\psi)_{\Omega} \xrightarrow{\text{PI.}} (\nabla w, \nabla\psi)_{\Omega} - (w, \nabla\psi \cdot \mathbf{n})_{\Gamma_{fs}} &= 0 && \text{on } \Omega \text{ (Mass conservation)} \\ (w, \psi_{,t} + g\eta)_{\Gamma_{fs}} &= 0 && \text{on } \Gamma_{fs} \text{ (dynamic B.C.)} \end{aligned}$$

In [1], this weak formulation is presented in the following way: *given* $g \in \mathbb{R}$, *find* $(\psi, \eta) \in \mathcal{W} \times \mathcal{V}$, such that for all $(w, v) \in \mathcal{W} \times \mathcal{V}$

$$B_l(\{w, v\}; \{\psi, \eta\}) = 0 \quad (3.5)$$

, with

$$B_l(\{w, v\}; \{\psi, \eta\}) = (\nabla w, \nabla\psi)_{\Omega} - (w, \eta_{,t})_{\Gamma_{fs}} + \frac{1}{2} \left(v + \frac{\alpha}{g} w, \psi_{,t} + g\eta \right)_{\Gamma_{fs}} \quad (3.6)$$

The added $\alpha \cdot w/g$ term guarantees coercivity by selecting α based on the time integrator. Coercivity ensures stability. Derivation of a coercivity statement for the non-linear case is beyond the scope of this thesis.

Energy evolution Akkerman and ten Eikelder [1] show energy conservation by selecting a case where $w = \psi_t$ and $v = 2\eta_t - \alpha\psi_t/g$. The weak formulation is rewritten and by use of the chain rule the definitions of the kinetic and potential energy are found.

$$\begin{aligned} B(\{w, v\}; \{\psi, \eta\}) &= (\nabla\psi_t, \nabla\psi) - (\psi_t, \eta_t)_{\Gamma_{fs}} + \frac{1}{2} \left(2\eta_t - \frac{\alpha}{g}\psi_t + \frac{\alpha}{g}\psi_t, \psi_t + g\eta \right) \\ &= (\nabla\psi_t, \nabla\psi)_{\Omega} + g(\eta_t, \eta)_{\Gamma_{fs}} \\ &= \frac{d}{dt} E_{kin} + \frac{d}{dt} E_{pot} = 0 \end{aligned}$$

Non-linear wave

Strong form The strong form is now complemented with non-linear terms:

$$\begin{aligned} \nabla^2\psi &= 0 && \text{on } \Omega \text{ (Mass conservation)} \\ \psi_{,t} + \frac{1}{2} |\nabla\psi|^2 + g\eta &= 0 && \text{on } \Gamma_{fs} \text{ (dynamic B.C.)} \\ \eta_{,t} + \psi_{,x}\eta_{,x} + \psi_{,y}\eta_{,y} - \psi_{,z} &= 0 && \text{on } \Gamma_{fs} \text{ (kinematic B.C.)} \\ \nabla\psi \cdot \mathbf{n} &= 0 && \text{on } \Gamma \setminus (\Gamma_{fs} \cup \Gamma_R) \end{aligned}$$

Weak form For the non-linear case, a similar approach is adopted for the interior. The kinematic boundary condition can be substituted into the arising boundary terms after integration by parts of the mass conservation equation. The dynamic boundary condition is multiplied by the test function γv to satisfy correct energy evolution.

$$\begin{aligned} -(w, \Delta\psi) \xrightarrow{P.I.} &= (\nabla w, \nabla\psi)_{\Omega(t)} - (w, \nabla\psi \cdot \mathbf{n})_{\Gamma_{fs}(t)} = (\nabla w, \nabla\psi)_{\Omega} - (w, \gamma\eta_{,t})_{\Gamma_{fs}(t)} && = 0 \\ & \left(\gamma v, \psi_{,t} + \frac{1}{2} \|\nabla\psi\|^2 + g\eta \right)_{\Gamma_{fs}(t)} && = 0 \end{aligned}$$

The weak formulation reads: *given* $g \in \mathbb{R}$, *find* $(\psi, \eta) \in \mathcal{W} \times \mathcal{W}$, such that for all $(w, \gamma v) \in \mathcal{W} \times \mathcal{W}$,

$$B_{nl}(\{w, v\}; \{\psi, \eta\}) = 0 \quad (3.7)$$

with

$$B_{nl}(\{w, v\}; \{\psi, \eta\}) = (\nabla w, \nabla\psi)_{\Omega(t)} - (w, \gamma\eta_{,t})_{\Gamma_{fs}(t)} + \left(\gamma v, \psi_{,t} + \frac{1}{2} \|\nabla\psi\|^2 + g\eta \right)_{\Gamma_{fs}(t)}$$

Energy evolution For the energy evolution we adopt the test function spaces to be $w = \psi_{,t}$ and $v = \eta_{,t}$. It is not possible to take the time derivative out of the integral analogous to the linearised case in [1]. This is due to the time dependent domain. The mass conservation term is rewritten using Reynold's Transport Theorem and the identities in equation (3.4):

$$\begin{aligned} \int_{\Omega(t)} \nabla(\psi_{,t}) \cdot \nabla\psi \, d\Omega &= \frac{d}{dt} \int_{\Omega(t)} \frac{1}{2} \|\nabla\psi\|^2 \, d\Omega - \int_{\Gamma_{fs}(t)} \frac{1}{2} \|\nabla\psi\|^2 \mathbf{u} \cdot \mathbf{n} \, d\Gamma \\ &= \frac{d}{dt} \int_{\Omega(t)} \frac{1}{2} \|\nabla\psi\|^2 \, d\Omega - \int_{\Gamma_{fs}(t)} \frac{1}{2} \|\nabla\psi\|^2 \gamma\eta_{,t} \, d\Gamma \end{aligned}$$

Substitution in the mass conservation term in equation (3.7) yields

$$\frac{d}{dt} \int_{\Omega(t)} \frac{1}{2} \|\nabla\psi\|^2 \, d\Omega + g \int_{\Gamma_{fs}(t)} \eta\gamma\eta_{,t} \, d\Gamma = 0.$$

Clearly, the first term is the kinetic energy evolution. We will now show that the second term equates to the potential energy. Applying Reynold's transport Theorem to the potential energy (equation (B.4))

$$\begin{aligned} \frac{d}{dt} \int_{\Omega(t)} gz d\Omega &= g \int_{\Omega(t)} \frac{\partial z}{\partial t} d\Omega + g \int_{\Gamma_{fs}(t)} z \mathbf{u} \cdot \mathbf{n} d\Gamma \\ & \left. z \right|_{\Gamma_{fs}} = \eta, \quad \mathbf{u} \cdot \mathbf{n} = \gamma \eta_{,t} \\ & \Rightarrow g \int_{\Gamma_{fs}(t)} \eta \gamma \eta_{,t} d\Gamma \end{aligned}$$

shows *total conserved energy evolution*

$$\begin{aligned} \frac{d}{dt} (E_{kin} + E_{pot}) &= \frac{d}{dt} \int_{\Omega(t)} \frac{1}{2} \|\mathbf{u}\|^2 + \frac{d}{dt} \int_{\Omega(t)} gz d\Omega \\ \frac{d}{dt} (E_{kin} + E_{pot}) &= \frac{d}{dt} \int_{\Omega(t)} \frac{1}{2} \|\nabla \psi\|^2 d\Omega + g \int_{\Gamma_{fs}(t)} \eta \gamma \eta_{,t} d\Gamma = 0 \end{aligned} \quad (3.8)$$

Discretization

The presented weak forms are also called variational forms of the governing PDE's. Approximation takes place when the weak form is discretized. Numerical discretization is done by partitioning the continuous domain Ω into a discrete subset and approximate the continuous solution space and test function space by a weighted sum of shape functions

$$\phi \approx \phi^h(x) = \sum_{e=0}^{n_{dof}} \phi_e N_e(x) \quad (3.9)$$

where the weights ϕ_e are called *Degrees Of Freedom* and

$$N_e(x) = \begin{cases} N(x), & x \in \Omega_e \\ 0, & x \notin \Omega_e \end{cases} \quad (3.10)$$

The continuous domain Ω relates to Ω_e by

$$\Omega = \bigcup_e \Omega_e \quad \bigcap_e \Omega_e = \emptyset$$

This approximation is applied to both the weighting functions as well as the solution function. For each term we can substitute these expressions in the weak form leading to an expression for each element e . The linear case from Akkerman et al. [2] for an element e is given by

$$B(\{w, v\}; \{\psi, \eta\}) = \sum_{j=0}^{n_{dof}} \left\{ (\nabla N_a^1, \nabla N_b \psi_j)_{\Omega_i} - (N_a^1, N_b \eta_{j,t})_{\Gamma_{i,fs}} + \frac{1}{2} \left(\frac{\alpha}{g} N_a^1 + N_a^2, N_b (\phi_{j,t} + g \eta_j) \right)_{\Gamma_{i,fs}} \right\}$$

The superscripts for the N_a basis functions denote the different finite element spaces. The parameter for α to guarantee coercivity with *midpoint time integration* is $\Delta t/2$.

The semi-discrete weak form can now be solved for the unknown time derivatives with appropriate initial and boundary conditions. The Method Of Lines is used to advance the solution in time.

3.3. Numerical model: time

The Method of Lines is applied to the semi-discrete system of equations. Semi-discrete in the sense that space is discretized using the Finite Element Method discussed in section 3.2. This system which solves for the continuous unknown time derivative $\phi_{,t}$ is treated as an ODE. The solution is advanced in time by integrating this ODE with a numerical integration method. We can define the time derivative to be a function of time and the solution.

$$\begin{aligned} \phi_{,t} &= f(t, \phi) \\ \phi^{n+1} &= \phi^n + \int_{t_n}^{t_{n+1}} f(t, \phi) dt. \end{aligned}$$

The integral is discretized with a method of choice, either implicit or explicit. As an example we will illustrate this by the midpoint method. The midpoint method evaluates the slope at the center of an interval $\Delta t = [t_n, t_{n+1}]$. Multiplication of this slope by the timestep Δt retrieves the solution at t_{n+1}

$$\int_{t_n}^{t_{n+1}} f(t, \phi) dt \approx \Delta t f(t^n + h, \phi^n + hk)$$

with $h = \Delta t/2$ for the implicit midpoint method. For the residual, a matrix vector computation of the form

$$\begin{aligned} F(\phi^h, \phi_{,t}^h, t) &= G(\phi^h, t) \\ \phi^h &= \{\psi^h, \eta^h\} \\ \phi_{,t}^h &= \{\psi_{,t}^h, \eta_{,t}^h\} \end{aligned} \quad (3.11)$$

is solved for $\phi_{,t}$. Here, the operators F and G are the semi-discrete counterparts of the weak form [4]. Initial conditions are set by means of a projection

$$F(\phi^h - \phi, 0, 0) = 0$$

Equation 3.11 is implicit when $G = 0$. The implicit midpoint method solves

$$F\left(\phi^h + \frac{\Delta t}{2}\phi_{,t}^h, \phi_{,t}^h, t + \frac{\Delta t}{2}\right) = 0 \quad (3.12)$$

for $\phi_{,t}$. By default the rate $\phi_{,t}$ is assumed to be non-linear. To accommodate this, a Newton-Raphson iteration scheme is used to approximate the rate at the new timestep.

$$\Delta\phi_{,t}^n = -J_F(\phi^n, \phi_{,t}^n, t^n)^{-1} F(\phi^n, \phi_{,t}^n, t^n) \quad (3.13)$$

Here, J_F is the Jacobian of the discretized equation.

$$J_F = \frac{\partial F}{\partial \phi}$$

Where the chain rule is applied to $\phi_{,t}$ and $\phi_{,x}$

$$f(\phi_{,t}, \phi) = \frac{1}{\Delta t} f(\phi), \phi \quad \text{and} \quad f(\phi_{,x}, \phi) = N_{,x} f(\phi), \phi \quad (3.14)$$

The increment $\Delta\phi_{,t}^n$ is then used to update the rate. This process repeats until either the absolute or relative residual reaches a certain convergence criteria. The resulting increment is added to the current rate. The new rate times Δt advances the solution in time.

3.4. Numerical model: Mesh motion

For the Non-linear case, the free-surface elevation is no longer linearised around the still water level. As such, it is required to update the mesh at every time-step. More specifically, for every Newton iteration the mesh has to be updated. Taking the non-linear weak form (3.7)

$$B = \int_{\Omega(t)} \nabla w \nabla \psi d\Omega - \int_{\Gamma(t)} w \gamma \eta_{,t} d\Gamma_{fs} + \int_{\Gamma(t)} v \gamma \left(\psi_{,t} + \frac{1}{2} \|\nabla \psi\|^2 + g\eta \right) d\Gamma_{fs}$$

η can directly be used to move the mesh. For the interior a uni-directional Poisson problem is assumed for η with $\eta|_{z=0} = 0$.

$$\int_{\Omega(t)} \kappa \frac{\partial^2 \eta}{\partial y^2} d\Omega = 0 \quad (3.15)$$

In every time-step we solve for the rate $\phi_{,t}$. Prior to the mesh update we need an update of the solution by means of

$$\phi^{n+1} = \phi^n + \Delta t \phi_{,t}^n \quad (3.16)$$

The solution of the free surface elevation can then directly be used to accommodate for the mesh motion by updating the DOF's. For each DOF i we get

$$\begin{bmatrix} x_i^{n+1} \\ y_i^{n+1} \end{bmatrix} = \begin{bmatrix} x_i^0 \\ y_i^0 \end{bmatrix} + \begin{bmatrix} 0 \\ \eta_i^n \end{bmatrix} \quad (3.17)$$

when $d = 2$.

3.5. Arbitrary Lagrangian Eulerian (ALE) Frame

The nodal values for a function ϕ now have to be corrected for the mesh motion, due to the movement of each node at every time step. Let us denote at each time t a point x on the deformed domain, which relates to a point X on the reference domain

$$x = x(X, t) \quad X \in \Omega_0, \quad x \in \Omega(t)$$

The time derivative of this function in the ALE frame is then defined to be

$$\left. \frac{\partial \phi}{\partial t} \right|_X = \left. \frac{\partial \phi}{\partial t} \right|_x + \mathbf{u} \cdot \nabla_x \phi$$

With \mathbf{u} being the mesh motion, the vertical mesh motion is equal to $\frac{\partial \psi}{\partial z}$, due to $\nabla \phi = \mathbf{u}$. In our case we incorporate a vertical mesh motion only. The time derivative in the Eulerian frame is then

$$\left. \frac{\partial \psi}{\partial t} \right|_x = \left. \frac{\partial \psi}{\partial t} \right|_X - \frac{\partial \psi^2}{\partial z} \quad (3.18)$$

It is argued that due to η being effectively being defined on a constant plane we need not to implement this. When implementing a wave maker boundary condition this does need to be implemented. We substitute the Lagrangian definition for ψ into the momentum equation yielding

$$B_{nl} = \int_{\Omega(t)} \nabla w \nabla \psi d\Omega - \int_{\Gamma(t)} w \gamma \eta_{,t} d\Gamma_{fs} + \int_{\Gamma(t)} v \gamma \left(\left. \frac{\partial \psi}{\partial t} \right|_X + \frac{1}{2} \|\tilde{\nabla} \psi\|^2 - \frac{1}{2} \frac{\partial \psi^2}{\partial z} + g\eta \right) d\Gamma_{fs}$$

$$\tilde{\nabla} = \left[\frac{\partial}{\partial x} \quad \frac{\partial}{\partial y} \right]^T$$

4

Tools: DelFI & MFEM

This chapter serves as a succinct introduction into DelFI and MFEM. This, to allow reproducibility of the work outlined in this thesis. First a global summary is given of the specifications of DelFI. Next, a step-by-step approach illustrates the implementation of a generic variational form into DelFI.

DelFI stands for Delft Finite Elements and IsoGeometric Analysis. DelFI is a wrapper for the FEM library MFEM [4]. MFEM stands for Modular Finite Element Method. In MFEM, the inherent topological hierarchy present in FEM is inherited into the library. Clever use of Object Oriented Programming clearly shows when FEM Objects are addressed vs. Linear algebra objects graphically shown in Figure 10. This abstraction of the construction of Linear algebra objects given a Finite Element formulation, allows for scalable support of distributed memory architectures. In this manner, any local group of element related operations can be executed on a per node basis.

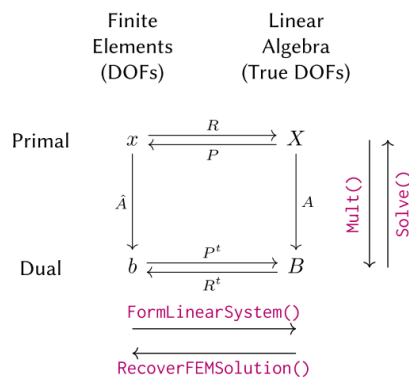


Figure 10: Relationship between FEM objects and linear algebra objects. From [4].

Secondly, MFEM also makes use of the compact support of FEM allowing for a partitioning of the domain and allocating each partition to a separate MPI rank. This MPI rank can then be allocated to a CPU or thread. Using this property, MFEM ensures nearly seamless scalability. Additional speed-up can be achieved by decomposing the local level operator to a element level and quadrature level operator in conjunction with the systems GPU. As of yet, this isn't implemented in DelFI. Transforming the DOF vector by using these operators is illustrated in Figure 11.

MFEM creates an abstract relation between two mathematical concepts: The Finite Element Method and Linear Algebra. DelFI extends this relation by distinguishing between physics and mathematics. In Chapter 3 a clear distinction is made between the physical model and numerical model and what laws have to be inherited by the numerical model. DelFI standardizes the numerical model allowing versatility in different physics implementations.

In DelFI, variational forms of transport equations such as the Navier Stokes equations or the Advection Diffusion equation can be implemented. The default assumes a single mesh with fixed boundary conditions.

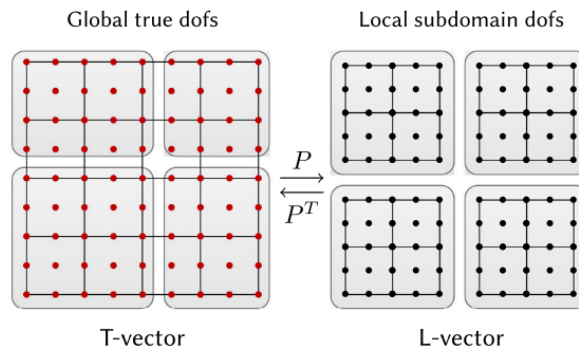


Figure 11: Graphic representation of decomposition of the DOF Vectors in the computational domain. The T-Vector corresponds to the linear algebra setting with X and B in Figure 10. . From [4]

Equivalently, a single mesh is used as input. In DelFI the Method Of Lines is implemented where a FEM spatial discretization is augmented by an ODE integration in time. Stabilization can be done through SUPG and PSPG. When a suitable (semi-discrete) variational form is derived, implementation can be done through a new physics definition.

4.1. Mesh input

The residual is approximated by a weighted sum of shape functions where the spatially independent weights are the solution variables. The mesh on which the shape functions are defined is given by a `.mesh` file. In the `.mesh` file a few different "headers" are given (Appendix E.1) followed by the mesh type. In this case a NURBS mesh. First the finite element relevant data is given by `dimension`, `elements` and `boundary`. Next the topological data is defined through `edges`, `vertices`, `patches`, `knotvectors` another `dimension` and `controlpoints`.

The first `dimension` denotes the dimension of the mesh by an integer. Under the `elements` header, the number of elements is denoted followed by a sequence of integers. The first integer is an identifier for the element. The second denotes the geometry type: 1 for a segment, 3 for a square and 5 for a cube. The integers following denote which nodes belong to the element in a counter clockwise convention. Next, under the `boundary` header the boundaries are defined in a similar manner. A boundary has a dimension less than the dimension of the problem itself. Thus if we describe an element with a square, then the boundary has to be defined with a segment. The `edges` header describes the edges needed for the NURBS implementation. In a square element, opposing edges share the same knotvector and they also have the same directionality. This is indicated by the first integer followed by the starting and ending node. The `vertices` header describes the number of vertices.

Next the parametric space is defined for each individual NURBS patch or "element". This section is indicated by the header `patches`. A 2D NURBS patch is constructed from the span of two knotvectors indicated in the `knotvectors` section. Here the first index denotes the degree, the second denotes the number of control points followed by the knots and their placement in the parametric space. The `dimension` section denotes the dimension of the knotvectors. Lastly, the section `controlpoints` denotes the controlpoints with 3D coordinates required to map the NURBS patch from the parametric space to the physical space. A graphic representation of a 2D NURBS patch is shown in Figure 12. When a correct weak form is implemented and a mesh is constructed DelFI is ready to be compiled and compute.

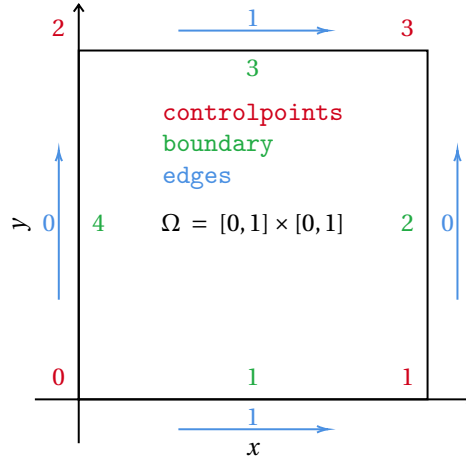


Figure 12: Graphic representation of the .mesh file for a unit square comprising of a single 2D surface element

4.2. Spatial discretization implementation

DelFI standardizes the weak form into a general residual statement. Each term of this form is defined in the `DELFI_Physics` class. Treatment of the interior Ω and boundary Γ is done separately. DelFI's spatial discretization is of the following

$$R = \sum_{k=1}^{v_{dim}} \left((N_k, I_A^k)_{\Omega} + (\nabla N_k, I_B^k)_{\Omega} + (N_k, I_C^k)_{\Gamma} + (\nabla N_k, I_D^k)_{\Gamma} \right) \quad (4.1)$$

$$= \sum_{k=1}^{v_{dim}} \left((N_k, I_{A0}^k)_{\Omega} + \sum_{i=1}^d \left(\frac{\partial N_k}{\partial x_i}, I_{Bi}^k \right)_{\Omega} + (N_k, I_{C0}^k)_{\Gamma} + \sum_{i=1}^d \left(\frac{\partial N_k}{\partial x_i}, I_{Di}^k \right)_{\Gamma} \right) \quad (4.2)$$

Where the residual R is minimized at a time t . This is the equivalent of the operator F given in section 3.3. The physics terms have to be assigned to each of the integrands I_{A0}^j and I_{Ai}^k listed in equation (4.2). Initialization of the integrands can be done by following Table 2. The test function basis functions are denoted N_j and

Table 2: DelFI implementation of integrands

Value	DelFI equivalent
I_{A0}^k	<code>I0 [k]</code>
I_{Ai}^k	<code>Ii [i] (k)</code>

v_{dim} is the variable dimension. The integrands I_{A0} and I_{Ai} are a function of the solution vectors ϕ^h . DelFI has a separate definition for the time- and spatial derivative listed in Table 3. With k denoting the variable.

Table 3: DelFI implementation of Jacobians

Value	DelFI equivalent
ϕ^{hl}	<code>phi [1]</code>
ϕ_j^{hl}	<code>dphidx [j] [1]</code>
$\phi_{,t}^{hl}$	<code>dphidt [1]</code>

For instance, the potential ψ^h is assigned to `phi [0]`. The Jacobian J_F from equation (3.13) is computed by splitting it into four separate parts which have to be defined both for the interior and the boundary. Equation (4.3) lists the Jacobian for the interior. Instancing in DelFI is shown in Table 4

$$\frac{\partial R}{\partial \phi} \Big|_{\Omega} = \sum_{k=1}^{v_{dim}} \left(\left(N_k, \frac{\partial I^k}{\partial \phi} \right)_{\Omega} + \left(\nabla N_k, \frac{\partial I^k}{\partial \phi} \right)_{\Omega} \right) \quad (4.3)$$

The differentiation rules for the integrand I^j have to be followed according to equation (3.14) for ϕ, t . The $\nabla\phi$ terms are captured by a separate instance of the Jacobian, namely J_{0i} . Both the integrands and Jacobians are

Table 4: DelFI and mathematical syntax of Jacobian terms.

Value	Definition	DelFI equivalent
J_{00}^{kl}	$\frac{\partial I_0^k}{\partial \phi_l}$	J00(k,l)
J_{0i}^{kl}	$\frac{\partial I_0^k}{\partial \phi_{l,j}}$	J0i[j](k,l)
J_{i0}^{kl}	$\frac{\partial I_i^k}{\partial \phi_l}$	Ji0[i](k,l)
J_{ij}^{kl}	$\frac{\partial I_i^k}{\partial \phi_{l,j}}$	Jij[i+dim*j][k][l]

initialized in the `DELFI_Physics` class. A new physics type has to be defined for each different set of PDE's, i.e. physical model. This can be for instance the convection-diffusion equation or the Navier Stokes equations. For the linear wave case, this class is named `LinearWave`. Each different physics implementation has its own `.hpp` and `.cpp` file. Additionally, it inherits from the `DELFI_Physics` class. The boundary condition functions, forcing terms together with relevant coefficients are read from a separate `.c` file. Additionally, some global or local monitors can be defined which are written to a separate `.dat` file.

4.3. Output

DelFI currently offers three methods for checking the solution or changes to a physics formulation. When a run starts the user can pipe the run output to a log file with `| tee log` at the end of the run command. In the log file a list is given of the options used in the run, what type of mesh is used and the number of unknowns for each variable. At each time step it uses Newton's method to approximate the next time step. Here information is passed regarding the norm of the residuals. In between Newton-steps, the amount of iterations needed for the GMRES solver. This linear solver solves for the residual at each time step. The amount of Newton and GMRES iterations give an indication on the conditioning of the Jacobian and residual. Additionally, the convergence rate of the residuals also gives an indication on the stability of the system. If these norms monotonically decrease with every Newton step, then the method shows to be stable.

Values such as Kinetic or Potential energy are assigned to global monitors. These global monitors are of the form

$$\int_{\Omega} m(\mathbf{x}) d\Omega \text{ and } \int_{\Gamma} m(\mathbf{x}) d\Gamma \quad (4.4)$$

The solution field projected to the mesh is written to an `.mfem_root` file. This file can be read using Visit [12]. The DelFI source code can be found on github [3] with a valid TU Delft account.

4.4. Flow of control

In this section the flow of control for DelFI is presented in Figure 13. This serves as a bird's eye view of how the program is executed.

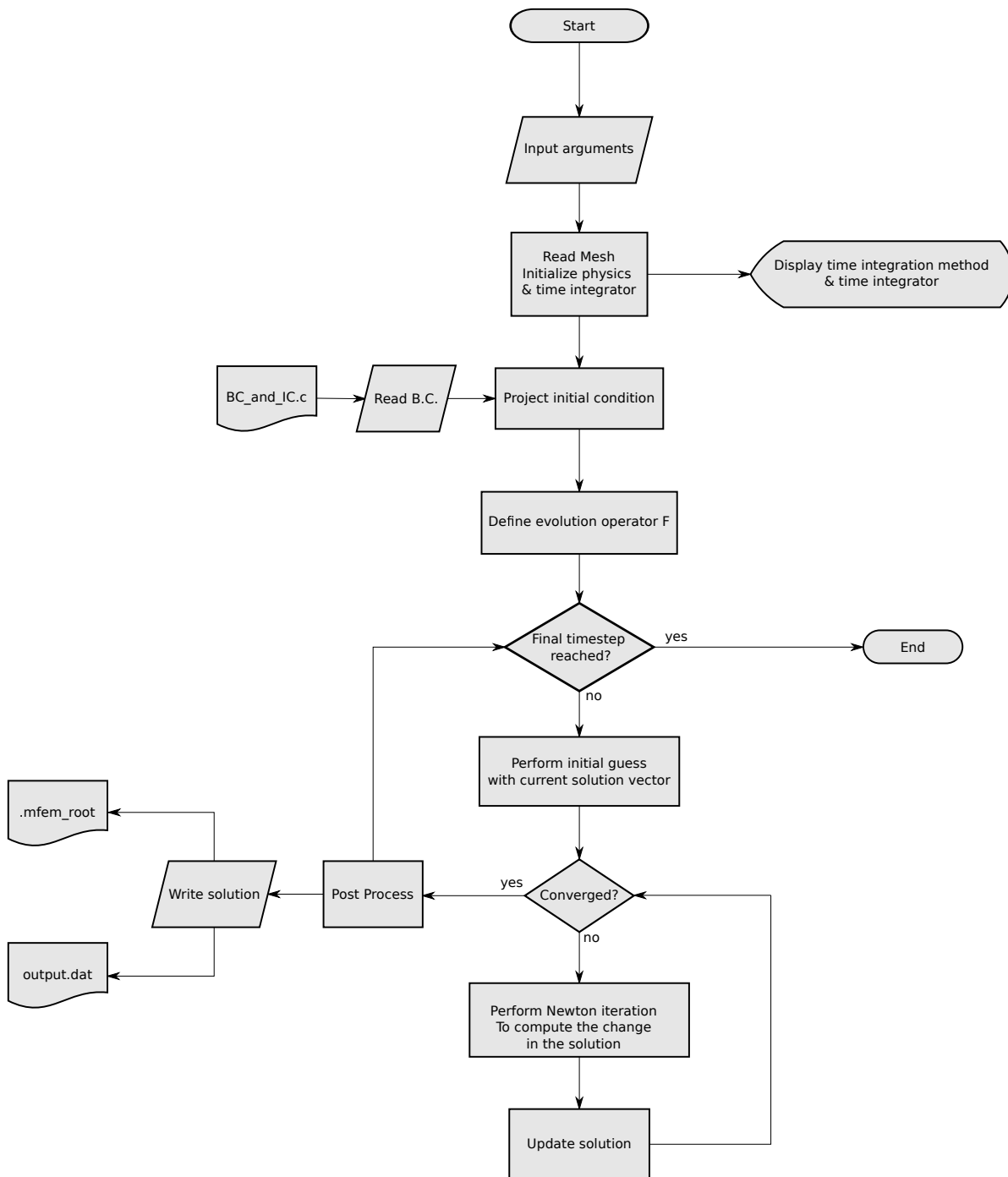


Figure 13: Flow of control for DelFI

5

Implementation: linear and non-linear wave

In chapter 3, a mathematical description of the wave problem is given and how the weak form is obtained from the governing equations. This results in a semi-discrete system of equations. Next, a method is presented to treat the weak form as an ODE which can be integrated in time. In chapter 4 DelFI, a program to approximate transport equations, is discussed. Here, the actions needed to implement a variational form are discussed. In this chapter we aim to apply this to the case of a linear and non-linear wave.

5.1. Linear wave

The linear form of the problem is presented in [2]. The weak form of the linear wave is given in equation (3.5). In [2] coercivity is obtained when $\alpha = 2/\Delta t = 1/dt$ for *midpoint time integration* where dt is the solver timestep passed in DelFI. Due to bilinearity (see appendix B.5), we can rewrite the weak form (3.5) into a form fit for implementation in DelFI

$$B(\{w, v\}; \{\psi, \eta\}) = (\nabla w, \nabla \psi) + \left(w, \frac{1}{\Delta t} \left(\frac{\psi_t}{g} + \eta \right) - \eta_t \right)_{\Gamma_{fs}} + \left(v, \frac{1}{2} (\psi_t + g\eta) \right)_{\Gamma_{fs}} \quad (5.1)$$

Verification is done according to an Airy wave with initial conditions

$$\begin{aligned} \eta_0 &= \eta_a \cos(kx) \\ \psi_0 &= \frac{\omega}{k} \eta_a \frac{\cosh(k(z+d))}{\sinh(kH)} \sin(kx) \end{aligned}$$

DelFI is limited in implementing this weak form. This is because η is not defined on the interior. The weak form has to be extended such that a non-zero value for η can be computed on the interior. A requirement is that these extra DOF's do not influence the boundary terms.

We introduce an "artificial anisotropic diffusion" to overcome DelFI's limitation. This artificial diffusion is defined to be

$$\kappa_y \frac{\partial^2 \eta}{\partial y^2} = 0 \quad \text{on } \Omega. \quad (5.2)$$

Requirements follow that the solution of actual problem given in equation (5.1) is not affected by this term. equation (5.2) shows that η on the interior is either constant or of constant slope. Two versions for implementing the free surface elevation η are presented. The first is to copy the initial condition η_0 from the free surface to the interior. The other is to multiply η with the y coordinate and setting Dirichlet conditions on the bottom.

Version A	Version B
$\eta_0^\Omega(x, y) = \eta_0$	$\eta_0^\Omega(x, y) = \eta_0 \cdot y$

Figure 14: Schematic representation of the different implementations of η for the interior.

5.1.1. Version A

The first option is relatively easy to implement as it requires no decoupling of the interior problem from the boundary problem. The strong form listed in Equation (5.2) is weighted by the test function space v . The boundary terms naturally drop out after integration by parts.

$$-\int_{\Omega} v \kappa_y \eta_{,yy} d\Omega = \int_{\Omega} v_{,y} \kappa_y \eta_{,y} d\Omega + \int_{\Gamma} v \kappa_y \eta_{,y} n_y d\Gamma \quad (5.3)$$

The weak form then becomes

$$B(\{w, v\}; \{\psi, \eta\}) = (\nabla w, \nabla \psi)_{\Omega} + (\nabla v, \kappa \circ \nabla \eta)_{\Omega} + \left(w, \frac{1}{2dt} \left(\frac{\psi_t}{g} + \eta \right) - \eta_t \right)_{\Gamma_{fs}} + \left(v, \frac{1}{2} (\psi_t + g\eta) \right)_{\Gamma_{fs}} \quad (5.4)$$

$$\kappa = \begin{bmatrix} 0 \\ a \end{bmatrix} \quad (5.5)$$

Following the conventions from chapter 4, the integrands are

$$I_i^0 = \psi_{,i}$$

$$I_i^1 = k_i \eta_{,i}$$

With the non-zero Jacobian terms

$$\frac{\partial I_i^0}{\partial \phi_{0,i}} = 1$$

$$\frac{\partial I_1^1}{\partial \phi_{1,1}} = a$$

For the boundary terms we have

$$I_0^0 = \frac{1}{2gdt} (\psi_t + g\eta) - \eta_t$$

$$I_0^1 = \frac{1}{2} (\psi_t + g\eta)$$

With the non-zero Jacobian terms

$$\frac{\partial I_0^0}{\partial \phi_0} = \frac{1}{2g(dt)^2}$$

$$\frac{\partial I_0^0}{\partial \phi_1} = \frac{-1}{2dt}$$

$$\frac{\partial I_0^1}{\partial \phi_0} = \frac{1}{2dt}$$

$$\frac{\partial I_0^1}{\partial \phi_1} = \frac{g}{2}$$

The initial conditions are defined in the `linearisedWave.c` file. We will highlight the initial condition for η as this differs between the two versions of the linearised cases. These are defined in separate functions for the exterior and interior.

When the weak form is implemented, the program has to be compiled. The flags `-bcp` and `-d99` have to be set to zero. These are flags that account for certain convergence criteria when dealing with viscous flows. As such, these criteria do not apply to potential flow. The Airy way is computed on a unit square mesh from appendix E.1. The waveheight and period are respectively $0.1 m$ and $1 m$.

5.1.2. Version B

For version B homogeneous Dirichlet conditions on the bottom are added to the unidirectional poisson problem. The natural boundary conditions that arise from integration by parts are no longer trivial. As a result, the interior problem needs to be decoupled from the boundary problem such that it does not affect the solution of ϕ and η on the boundary. Effectively we solve two problems. One is the wave problem and the other is a unidirectional Poisson problem with Dirichlet conditions on top and bottom.

$$\left. \frac{\partial^2 \eta^n}{\partial y^2} \right|_{\Omega} = 0 \quad (5.6)$$

$$\left. \eta^n \right|_{y=0} = 0 \quad (5.7)$$

$$\left. \eta^n \right|_{y=\eta} = \eta^n \quad (5.8)$$

Implementation of the weak form is the same as for version A. Changes have to be made to the `DELFI_Form` class. In this class the operators F and J are defined to solve for ϕ_t^h . This is done in two loops: one for the interior and one for the exterior. To decouple η from the interior we set the solution ϕ_t^h to be zero for the DOF's corresponding to the free-surface. Secondly, we have to set the rows of J to be equal to zero after the interior loop for the same DOF's. This decouples the problem in the Newton iteration. The total result is a one way coupling from the wave problem to the interior, but not vice versa. Because the boundary terms are accounted after the interior loop, these remain unaffected. The procedure is highlighted in Equation (5.9).

$$\begin{aligned} \Delta \begin{bmatrix} \phi, t|_{y=\eta} \\ \phi, t|_{y \neq \eta} \end{bmatrix} &= \Delta \begin{bmatrix} \phi, t|_{y=\eta} \\ \phi, t|_{y \neq \eta} \end{bmatrix}_{\Gamma} + \Delta \begin{bmatrix} \phi, t|_{y=\eta} \\ \phi, t|_{y \neq \eta} \end{bmatrix}_{\Omega} \\ \Delta \begin{bmatrix} \phi, t|_{y=\eta} \\ \phi, t|_{y \neq \eta} \end{bmatrix} &= - \begin{bmatrix} J_{00} & J_{01} \\ J_{10} & J_{11} \end{bmatrix}^{-1} \begin{bmatrix} F_{00} & F_{01} \\ F_{10} & F_{11} \end{bmatrix} \begin{bmatrix} \phi, t|_{y=\eta} \\ \phi, t|_{y \neq \eta} \end{bmatrix} \\ &= \left(\begin{bmatrix} J_{00} & J_{01} \\ J_{10} & J_{11} \end{bmatrix}_{\Gamma} + \begin{bmatrix} J_{00} & J_{01} \\ J_{10}^0 & J_{11}^0 \end{bmatrix}_{\Omega} \right)^{-1} \left(\begin{bmatrix} F_{00} & F_{01} \\ F_{10} & F_{11} \end{bmatrix}_{\Gamma} + \begin{bmatrix} E_{00}^0 & F_{01} \\ E_{10}^0 & F_{11} \end{bmatrix}_{\Omega} \right) \left(\begin{bmatrix} \phi, t|_{y=\eta} \\ \phi, t|_{y \neq \eta} \end{bmatrix}_{\Gamma} + \begin{bmatrix} \phi, t|_{y=\eta} \\ \phi, t|_{y \neq \eta} \end{bmatrix}_{\Omega}^0 \right) \end{aligned} \quad (5.9)$$

The main advantage of this formulation over the other is that no influence of the interior onto the boundary is guaranteed. Additionally, values of η on the interior can be directly used to incorporate mesh motion needed for the non-linear case. The method can be summarized in the following steps and is graphically shown in Figure 15:

1. Solve poisson on the interior with essential boundary condition for $\eta|_{\Gamma}$
2. "Turn off" essential boundary condition
3. Evaluate wave problem

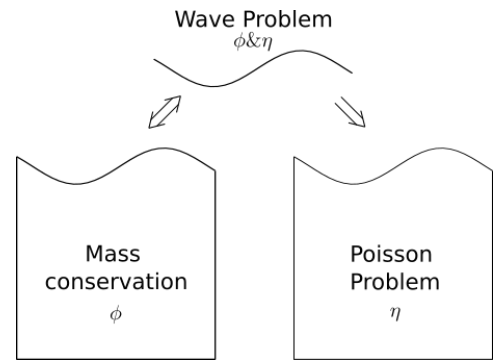


Figure 15: One way coupling of the Poisson problem

5.2. Non-linear wave

The variational form of the non-linear wave from equation 3.7 is reintroduced with the Jacobian γ on the righthandside of the comma and the additional term on the interior to solve for η

$$B_{nl}(\{w, v\}; \{\psi, \eta\}) = (\nabla w, \nabla \psi)_{\Omega(t)} + (\nabla v, \kappa \circ \nabla \eta)_{\Omega} - (w, \gamma \eta, t)_{\Gamma_{fs}(t)} + \left(v, \gamma \left(\frac{\partial \psi}{\partial t} + \frac{1}{2} \|\tilde{\nabla} \psi\|^2 - \frac{1}{2} \frac{\partial \psi^2}{\partial z} + g \eta \right) \right)_{\Gamma_{fs}(t)}$$

Implementing this in DelFI results in the non-zero integrands for the interior

$$\begin{aligned} I_i^0 &= \psi, i \\ I_i^1 &= k_i \eta, i \end{aligned}$$

With the non-zero Jacobian terms

$$\begin{aligned} \frac{\partial I_i^0}{\partial \phi_{0,l}} &= 1 \\ \frac{\partial I_i^1}{\partial \phi_{1,l}} &= k \end{aligned}$$

The boundary terms are

$$\begin{aligned} I_0^0 &= -\gamma \eta, t \\ I_0^1 &= \gamma \left(\frac{D\psi}{Dt} + \frac{1}{2} \|\tilde{\nabla} \psi\|^2 - \frac{1}{2} \frac{\partial \psi^2}{\partial z} + g \eta \right) \end{aligned}$$

With the Jacobian terms

$$\begin{aligned} \frac{\partial I_0^0}{\partial \phi_0} &= 0 \\ \frac{\partial I_0^0}{\partial \phi_1} &= -\frac{\gamma}{\Delta t} \\ \frac{\partial I_0^1}{\partial \phi_0} &= \frac{\gamma}{\Delta t} \\ \frac{\partial I_0^1}{\partial \phi_1} &= \gamma g \\ \frac{\partial I_0^1}{\partial \phi_{0,i}} &= \gamma \psi, i \quad i = \{0..d-1\} \\ \frac{\partial I_0^1}{\partial \phi_{0,d}} &= -\gamma \psi, d \end{aligned}$$

Here we assume the variable γ to be much less dominant than the other variables. Otherwise, this also has to be taken into account in the Jacobians as it is a function of η .

6

Results

This chapter presents the results obtained from the implementation of the linear and non-linear forms. First the two versions of the linear form are presented to demonstrate computation of a free-surface problem in DelFI and which one is correct. Next the non-linear wave is demonstrated for a simple unit square sloshing case. Lastly, we've validated the method against a DNV sloshing case where we compare the results with numerical results from others.

6.1. Linear Wave

The linear wave is validated and verified against an analytical Airy wave. The initial conditions are plotted in Figure 16, clearly showing the difference in how to treat the wave elevation η . The different versions are compared to each other with respect to the artificial diffusion parameter κ as well as conservation of mass and energy. Additionally, mesh convergence is also checked.

Table 5: Data corresponding to the linear test case.
These values follow the linear wave criterion from [20]

Variable	Value	Unit
Ω	$[0, 1] \times [0, 1]$	$m \times m$
η_a	0.1	m
k	6.28	m^{-1}
λ	1	m
ω	7.85	$rad \cdot s^{-1}$
T	0.8	s

6.1.1. Diffusivity dependence

The artificial diffusion is checked by plotting the total wave elevation and potential for an Airy wave for a set of diffusivities (Figure 17). If the method is computed correctly, no spurious behaviour should be observed in the results. With version A however, it can be observed that the total mean potential shows to have no consistent behaviour towards a higher diffusivity. In contrast version B does show to have consistent behaviour of ϕ and η with increasing diffusivity. The solution for ϕ and η does change with increasing diffusivity, even though the Poisson problem for η is numerically decoupled from the wave problem. This could be due to round off errors. The means converge towards machine precision for version B.

6.1.2. Mesh convergence

Mesh convergence is done to check if a numerical is consistent, that is the error decreases consistently with the data. For the linear mesh convergence, a similar method is adopted as Brink et al. [7]. The simulation for the Airy wave is run for 10 periods after which the mean absolute error between η^{Airy} and η^h is checked. This is done both for the degree (p-refinement) as well as the mesh size (h-refinement). In contrast to Akkerman et al. [2], the coarsest mesh is 4×3 DOF's. With less DOF's the amount of nodes in x direction is no longer

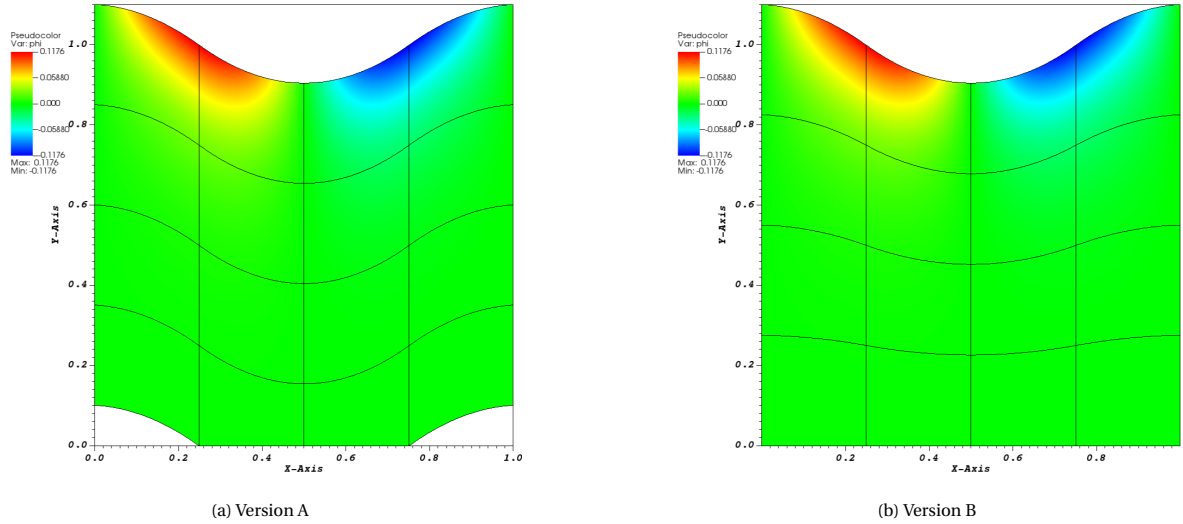


Figure 16: Initial conditions with quadratic NURBS for version A and B. The variable η is used to displace the mesh illustrating the difference between the two formulations. This mesh displacement is a feature of the Visualization software and not computed for the linearised case.

sufficient for the initial conditions to plot a cosine. A sine is possible, due to the shift in phase. In this case, the potential ϕ can no longer be fit accordingly. A solution to this could be to project the initial conditions for ϕ with the gradient of ϕ .

Table 6: Data corresponding to different mesh refinement strategies

(a) h-refinement		(b) p-refinement	
h-refinement	mesh size	p-refinement	Basis Function
$2^f \times 2^f$	$el_x \times el_y$	$p = 1$	Linear
		$p = 2$	Quadratic
		$p = 3$	Cubic

6.1.3. Energy convergence

As stated previously, Both the linear and the non-linear problem should be energy conservative. For the airy wave the wave energy is defined by

$$\frac{1}{2} g \zeta^2 \quad (6.1)$$

The energy evolution is plotted in Figure 25. Energy conservation shows to hold. Obviously, the energy convergence is directly linked to the wave elevation convergence.

6.1.4. Mass conservation

For mass conservation a sloshing case is checked with initial condition

$$\eta_0 = \eta_a \cos(kx). \quad (6.2)$$

The results of which are shown in Figure 22b and 27. Mass is not fully conserved. Yet when adopting sufficient mesh refinement we do converge towards mass conservation. The mass flux over the boundary does balance the mass change in the interior. These problems originate from an incorrect no-penetration boundary condition. It is believed that this is due to a bug in DelFI. Due to time restrictions we were unable to solve this. The mass flux over the free-surface does show to be consistent with the free-surface velocity with round-off errors in the range $\mathcal{O}(10^{-12})$.

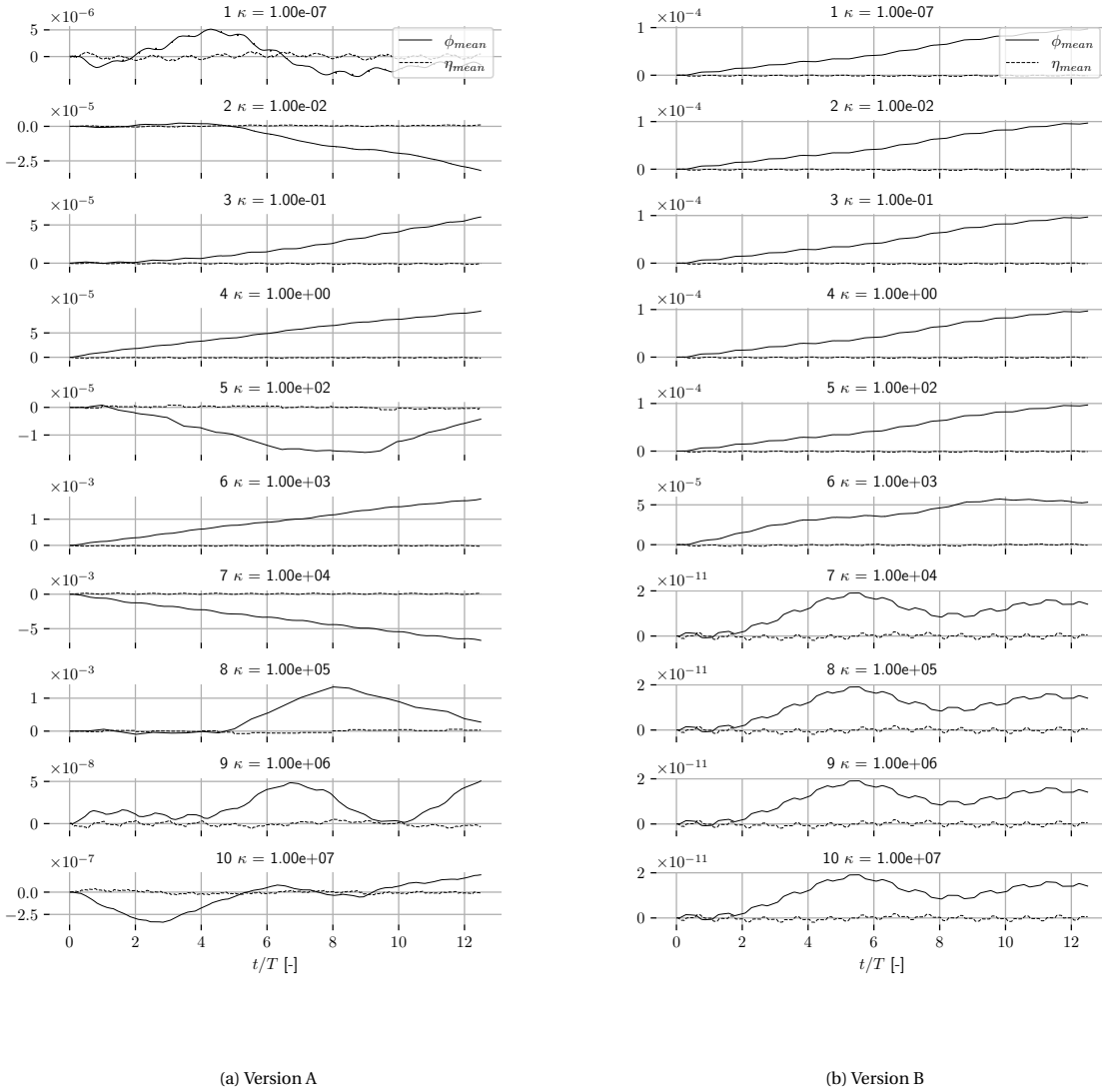
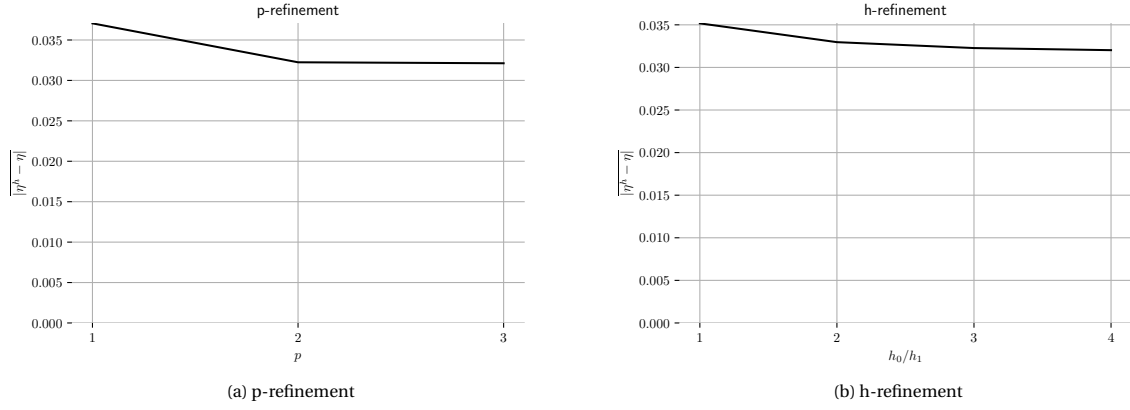
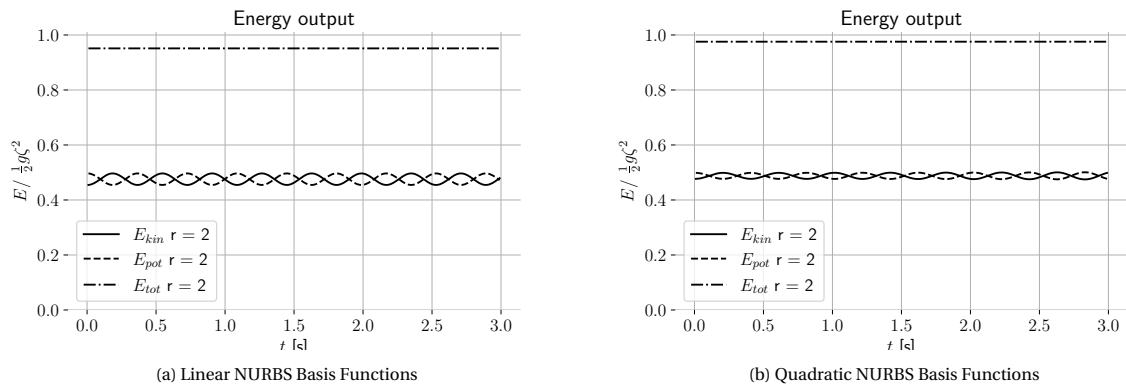
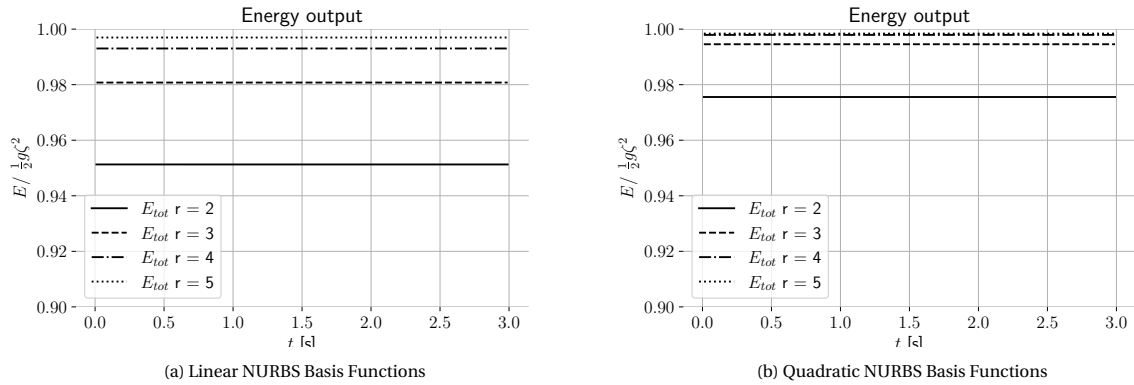


Figure 17: $\int_{\Omega} \eta d\Omega$ and $\int_{\Omega} \phi d\Omega$ with temporal resolution $dt/T = 0.125$ Spatial resolution $h/\lambda = 0.25$. Quadratic NURBS

6.1.5. Total potential and free surface

Furthermore, The total potential and free-surface are checked. Here, η remains stable around the horizontal axis, whereas ϕ shows no clear trend. When running longer computations the deviation remains within the order of $\mathcal{O}(10^{-11})$. The fact that ϕ shows no clear trend is that for the linear case the free-surface boundary condition is determined up to a constant.

Figure 18: p- and h- convergence of the error of the Airy wave profile η for version BFigure 19: Energy evolution for version B. $\Delta t = 0.01$ Figure 20: Total energy convergence for version B. The total energy is non-dimensionalized with respect to the analytical energy. $\Delta t = 0.01$

6.2. Non-linear wave

Benchmarks that could be easily validated for the Non-linear sloshing case were hard to obtain. Wilkening [42] does show a case for a non-linear Fourier expansion, but implementation of this method is rather tedious. In Brink et al. [7], a Fenton Rienecker wave is used as a benchmark. The code from which is publicly available at Fenton [16]. For a Fenton Rienecker we would need a periodic boundary condition similar to the linear Airy case.

A periodic boundary condition hasn't been implemented yet. As such, for validation we will use a DNV sloshing case from Westhuis [39]. First we will present the energy and mass results for the non-linear case.

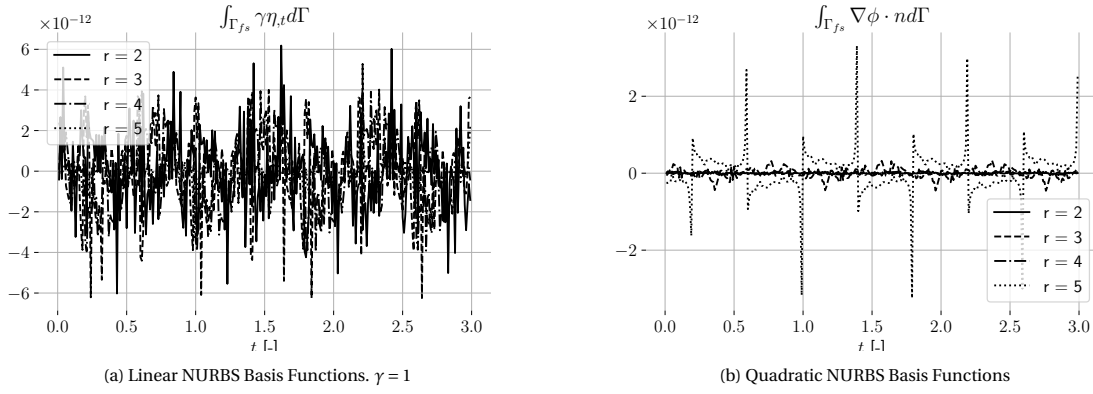


Figure 21: Free-surface flux. $\Delta t = 0.01$

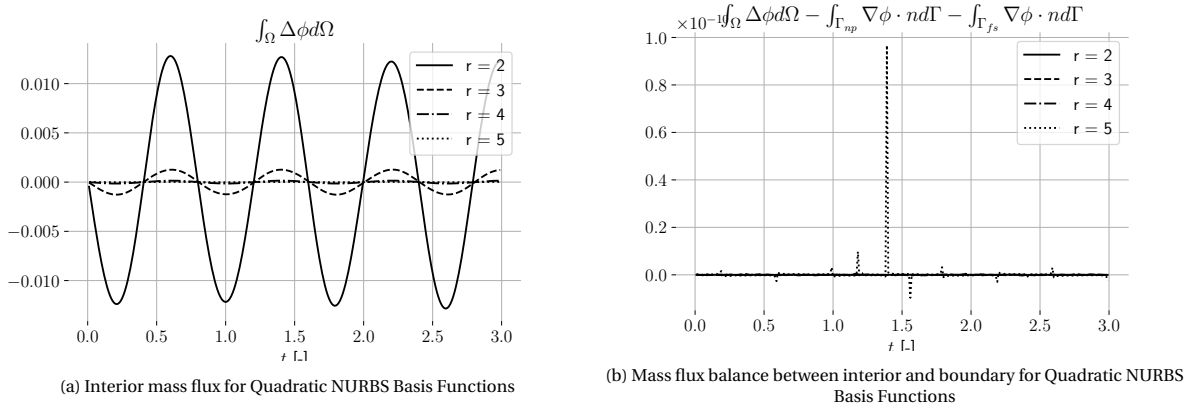


Figure 22: Mass flux statements for the standing waves. $\Delta t = 0.01$

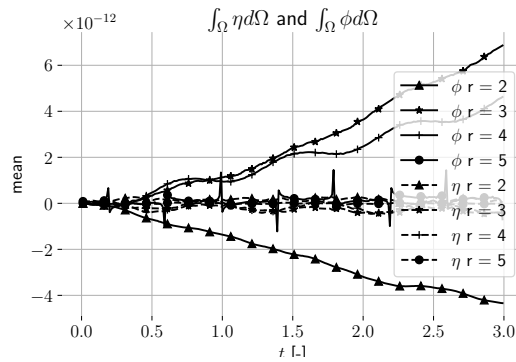


Figure 23: Mean global potential and free surface. $\Delta t = 0.01$

Data corresponding to this case is listed in Table 7. In Figure 24b we can see the additional effects captured in the non-linear case with respect to the linear case shown in Figure 24a.

Table 7: Data corresponding to the non-linear test case

Variable	Value	Unit
Ω	$[0, 1] \times [0, 1]$	$m \times m$
η_a	0.05	m

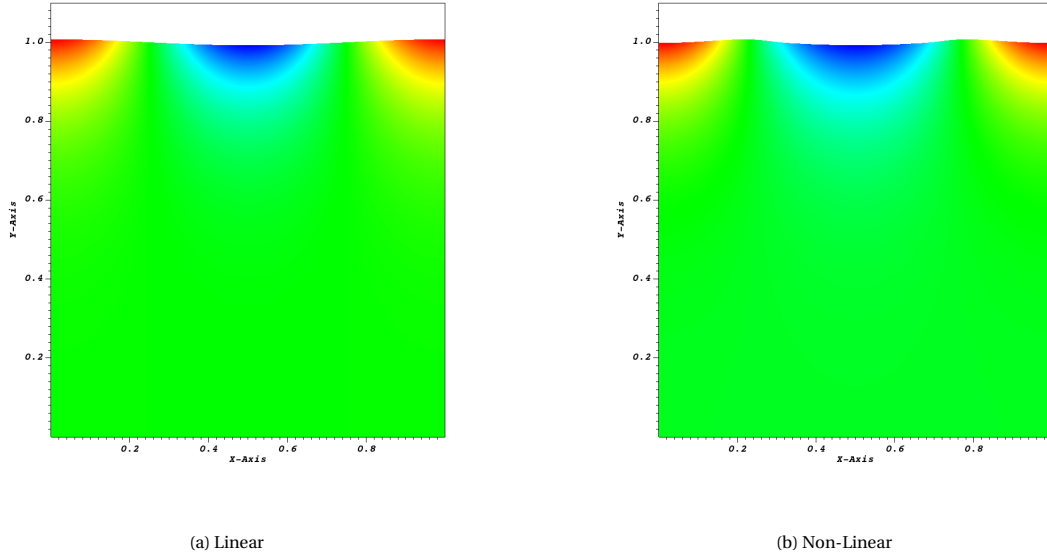


Figure 24: Snapshots of the sloshing standing wave at $t = 0.62[s]$. On the left for the linear formulation and on the right for the non linear formulation

6.2.1. Energy

The Energy is plotted for h- and p-refinement in Figure 25a and Figure 25b respectively. h-refinement is checked with Linear basis functions. In both Figures the energy is not conserved. Erratic behaviour can be detected by adopting h-refinement strategy. For p-refinement this is less clear. First of all for the waveheight of 0.05 instabilities occur when $p = 3$. By reducing the time resolution these instabilities are delayed. The cause of these instabilities is the higher density of nodes near the boundary when adopting p-refinement. Locally this increases the Péclet number and thus the solution becomes unstable. Still, we've derived that energy conservation should be satisfied. Two factors could be playing a role in this not being the case. One is the mass flux over the boundary shown in the linear case. The other is that the mapping from a Eulerian to a Lagrangian frame of reference was done incorrectly.

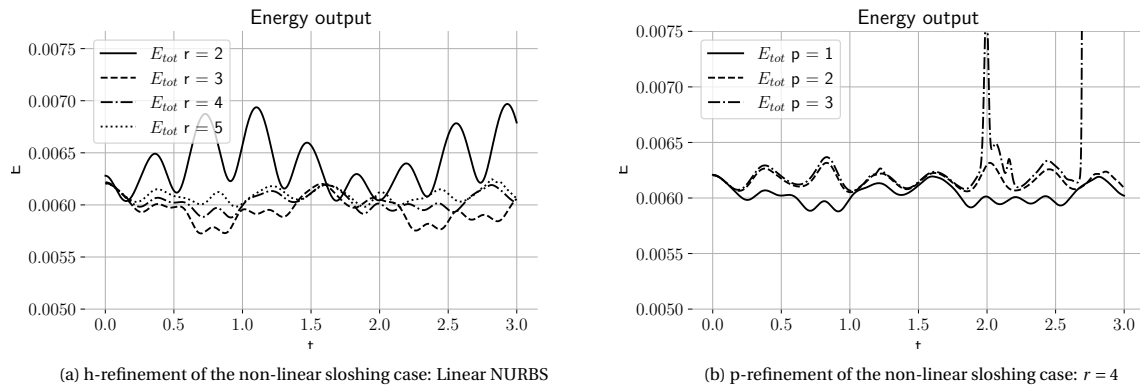
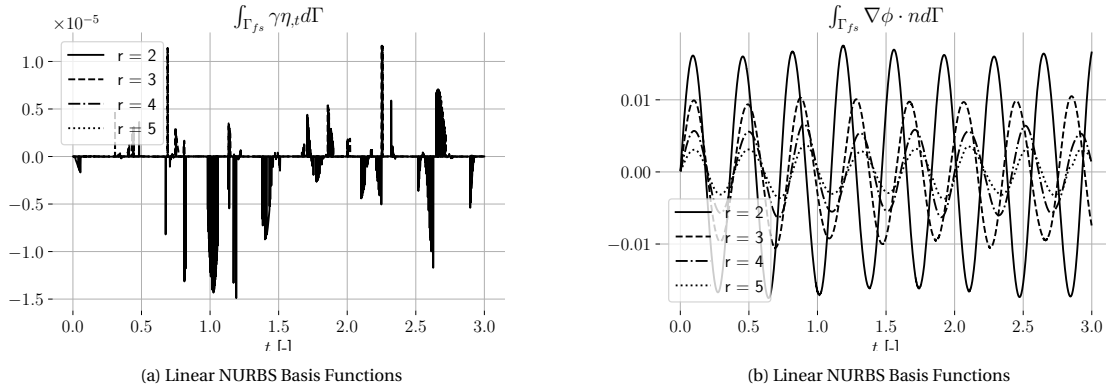


Figure 25: Energy evolution for the non-linear wave problem with different refinement strategies. $\Delta t = 0.001$

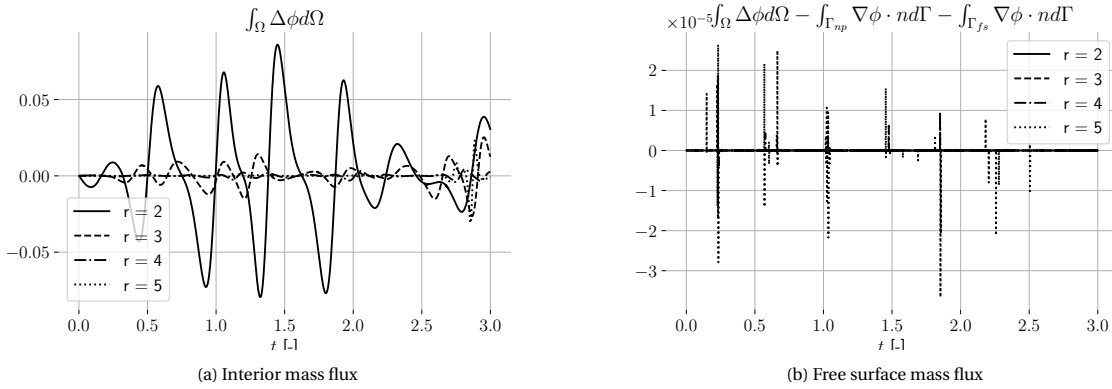
6.2.2. Mesh convergence

The kinematic free-surface condition shows to be within acceptable limits, implying conservation of the geometry. The mass flux over the free-surface reduces with mesh refinement. A phase shift is observed. For the coarsest mesh a second period is observed in the mass flux, which again reduces with mesh refinement.

Figure 26: Free-surface flux. $\Delta t = 0.001$

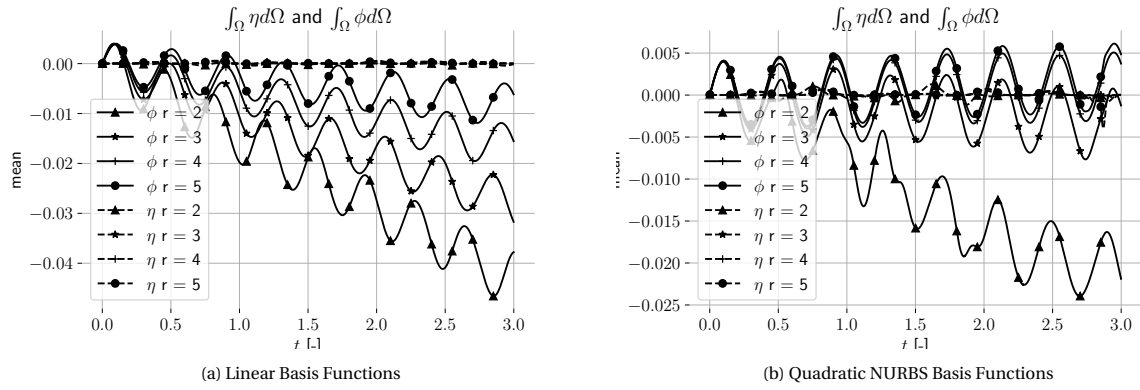
6.2.3. Mass conservation

Even though incompressibility is not achieved, but can be reduced with sufficient mesh refinement, mass is conserved. In Figure 27a the laplace equation for the potential is not satisfied with coarse meshes. This indicates that the fluid is not incompressible. Mass conservation is followed. Figure 27b indicates that divergence of mass in the interior equates to the mass flux over the boundary.

Figure 27: Mass balance Quadratic NURBS basis functions. $\Delta t = 0.001$

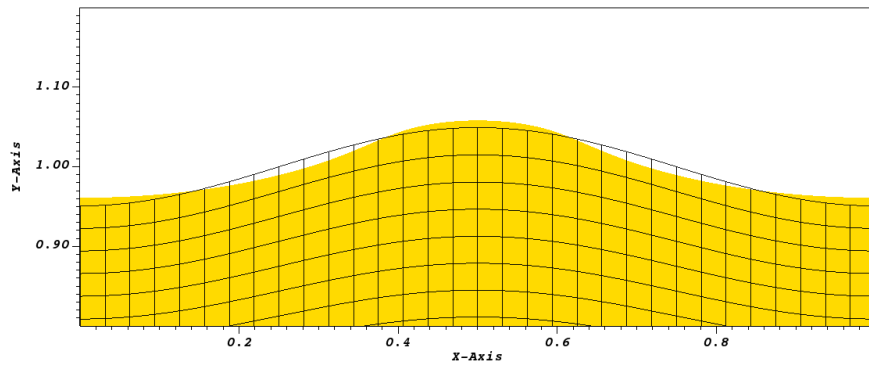
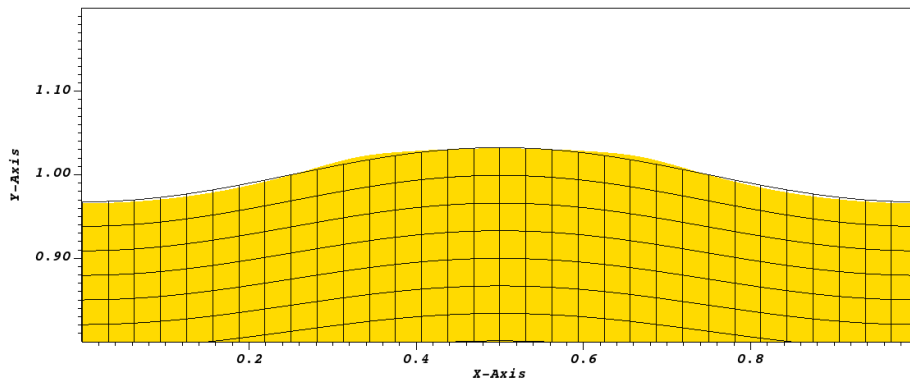
6.2.4. Total potential and free surface

The total potential and free-surface elevation converge with adequate mesh refinement. When adopting higher order basis functions the solution is observed to be more prone to instabilities. When adopting a p-refinement strategy additional degree's of freedom are also inserted. A clustering of these nodes occurs at the boundaries and this locally decreases the mesh width significantly [21]. The result could be an increase in the Local Péclet number and resulting in instabilities. Due to no physical stabilisation in the form of viscosity or free-surface tension or any stabilization scheme such as SUPG[9].

Figure 28: Free-surface flux. $\Delta t = 0.001$

6.2.5. Comparison of linear free surface with non-linear free surface

In Figure 29 and 30 a close up of the linear and non-linear free surface is displayed. The shallower trough and higher peak is clearly observed for the non-linear case. A feature which is also observed in the second order Stokes waves. A couple of time instances later we can see that the crest has actually flattened out. Also known as a dimpled crest [20]

Figure 29: Close up of the free surface for the linear case indicated by the grid. The non-linear free surface is shown with the filled colour. $\Delta t = 0.001$ Figure 30: Dimpled crest where we can see that the crest is flattened out by collapsing under its own weight. $\Delta t = 0.001$

6.2.6. Case: Sloshing DNV

Lastly we validate the code against other results presented in Westhuis [39]. This is a numerical sloshing benchmark presented by DNV. In this case eight participants, including Westhuis [39] presented their findings on a sloshing case where the initial free-surface is perturbed by

$$\eta_0(x, y) = \frac{12y}{70} (1 - (x/53)^2) e^{-(x/76)^2} \quad (6.3)$$

, which is graphically shown in Figure 31. Parameters of the Westhuis [39] case compared to ours are listed in Table 8.

Table 8: Data corresponding to the DNV sloshing benchmark.

Variable	This thesis	Westhuis [39]	Unit
Ω	160×70		$m \times m$
$DOF_x \times DOF_y$	35×36	160×15	–
Δt	0.1	0.1	s

Table 9 shows that our data comes close to the other data. Figure 32 shows the fluid state at this time. Realistic results can still be obtained, even though mass and energy conservation are not as reliable as is deemed optimal.

Table 9: Data corresponding to the DNV sloshing benchmark at $x = 60[m]$ and $t = 9.2[s]$. With \bar{X} and σ being the mean and standard deviation respectively. Our data is obtained from VisIt and may have some additional interpolation errors.

	$\eta[m]$	$u_x[m/s]$	$u_y[m/s]$
\bar{X}	-3.796	-2.4095	-0.535
Participant nr.			
1	-3.803	-2.456	-0.363
2	-3.860	-2.280	-0.560
3	-3.815	-2.414	-0.445
4	-3.759	-2.411	0.602
5	-3.820	-2.417	-0.580
6	-3.803	-2.417	-0.572
7	-3.720	-2.480	-0.690
Westhuis [39]	-3.788	-2.401	-0.561
This thesis	-3.795	-2.449	-0.501

Table 10: Deviation from the mean listed in Table 9. Data corresponding to the DNV sloshing benchmark at $x = 60[m]$ and $t = 9.2[s]$. Our data is obtained from VisIt and may have some additional interpolation errors.

Participant nr.	$\eta[\%]$	$u_x[\%]$	$u_y[\%]$
1	-0.1873	-1.745	32.97
2	-1.689	5.547	-3.406
3	-0.5035	-0.004603	17.83
4	0.9718	0.1197	-11.16
5	-0.6352	-0.1289	-7.099
6	-0.1873	-0.1289	-5.622
7	1.999	-2.739	-27.41
Westhuis [39]	0.2078	0.5339	-3.59
This thesis	0.02342	-1.455	7.489

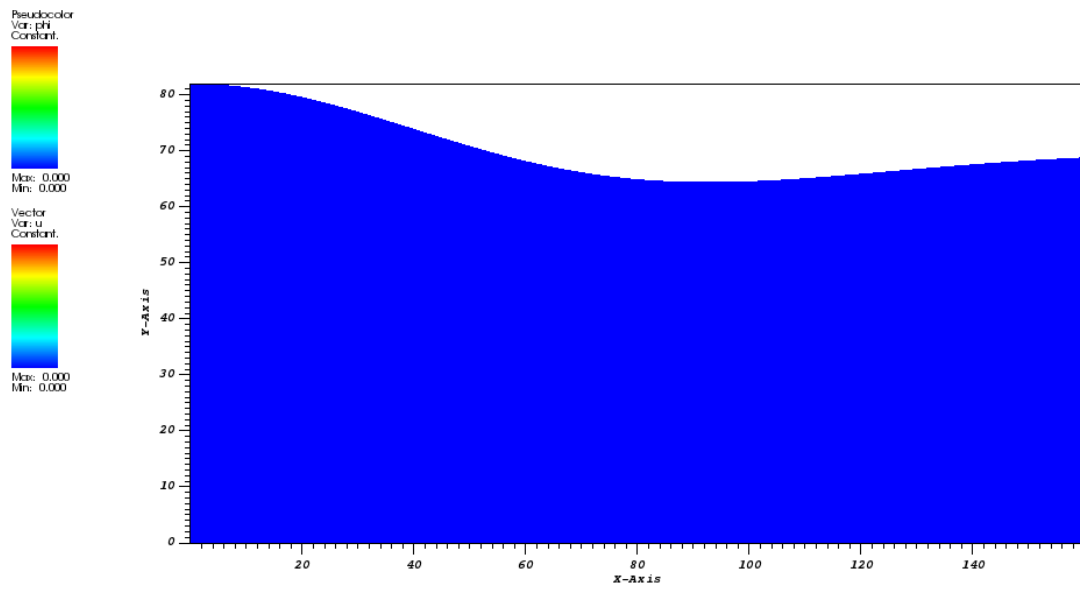


Figure 31: Initial conditions from DNV sloshing case. The initial condition for the free surface is captured in the mesh deformation.

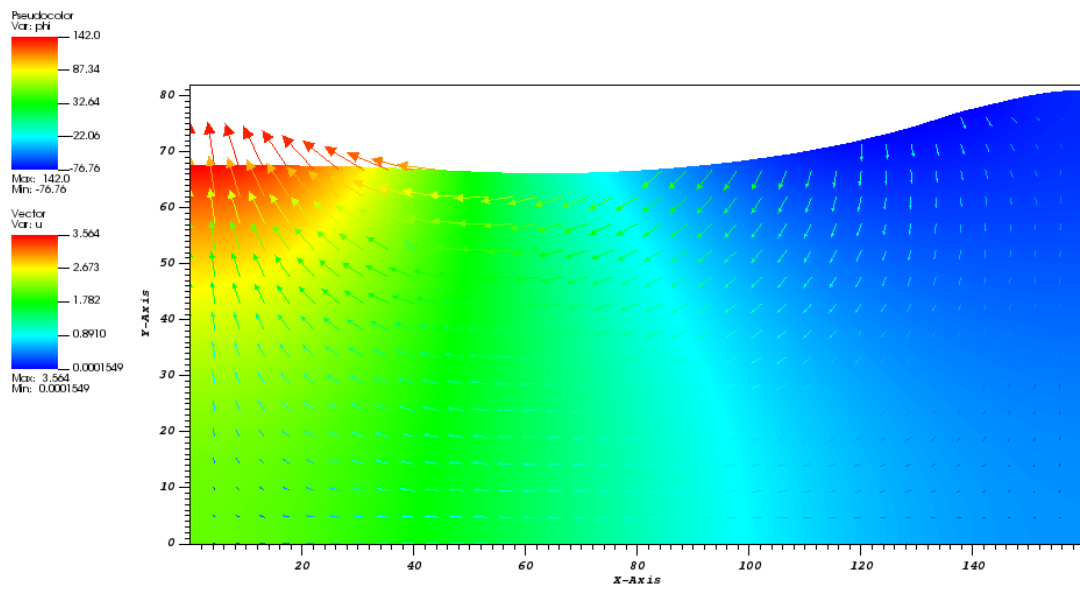


Figure 32: Solution at $t = 9.2$ from DNV sloshing case. The colormesh denotes the potential and the vectorplot the velocities.

7

Conclusions & recommendations

The ability to develop a flexible and open-source method which could optimize towards a given wave-maker input given a certain free-surface profile is necessary. Adopting such an iterative method in the towing tank itself provides too costly of a method. This motivated strongly for the development of an in-house numerical method which proved to be *accurate, stable* and *fast*. To achieve this:

- A suitable physical model had to be adopted where accuracy had to be balanced with simplicity
- The numerical model and the physical model need to inherit the same properties.
- The numerical method has to be fast which is inevitably highly dependent on the tools in which it is implemented. Reproducibility requires the need to use open-source software where every detail is documented
- Added features in the tools had to be consistent with the mathematical framework. Careful documentation ensures that the fellow scholar can fill the missing pieces.
- Results have to be analysed and flaws which were unsolvable in the given time frame need to be addressed. Suggestions can then be made for future work

7.1. Conclusion

A literature research provided a review of the state-of-the-art. A potential flow model proved to fit the requirements. It was shown that from these equations an integral extrema can be derived indicating the existence of a unique solution. It is argued that the reduced degrees of freedom in Boundary Element Methods is not necessarily advantageous over the Finite Element Method. The compact support of basis functions in FEM allows better use of the machine's architecture. Additionally, the more rigorous mathematical tool-set gives the ability to derive properties such as stability and accuracy. Properties that are difficult to prove in BEM. Literature further demonstrated that an energy conservative method is clearly superior over a non-conserving one. Enhancing conventional FEM with the Isogeometric Framework capped the literature research and requirements for the method were set.

Successful implementation of the method in DelFI shows this tool to be viable for use in this thesis. Computing a variable which is only defined on the boundary is achieved by extending it to the interior and effectively solving two problems. Herein the wave problem was coupled unidirectional to interior problem such that the wave problem remains unaffected. DelFI shows to be flexible enough to allow the implementation of a monolithic linear potential free-surface flow problem. This is shown by addressing the energy conservative properties of the numerical method together with different formulations of conservation of mass. The energy conservation shows to hold. Conservation of mass is not guaranteed, but can be reduced by adopting an appropriate space and time resolution. Validation against an Airy wave shows these errors to be marginal with respect to results achieved.

Extension to the non-linear case shows to have been conditionally successful. The added feature to compute a variable that is defined on the boundary alone is directly used for mesh deformation to capture non-linear effects. A sloshing case demonstrates the implementation of the non-linear potential flow equations

compared to others. Although only nodal values are evaluated, it does demonstrate that the method validates against others. Energy conservation is not guaranteed. Possibly this is due to the previous mass conservation error having a direct effect on the energy. A second argument could be that in the implementation of the integral not all Lagrangian definitions have been adequately implemented. Results also show that instabilities occur when using a p-refinement strategy. P-refinement introduces additional nodes near the boundary of the problem and hereby increasing the local Péclet number. The instabilities are observed most apparent near the boundaries. SUPG provides a solution method that complies with the research question.

Currently, results from conservation laws and instabilities that are a natural result of the method can be reduced with appropriate mesh and time resolution. Still, a DNV sloshing benchmark shows that the method is capable of reproducing the results of others with less degrees of freedom.

7.2. Recommendations

In this thesis a basis is laid for development of a digital twin of a towing tank. The main focus was the implementation of a novel variational form describing the non-linear potential flow equations.

Investigation of numerical behaviour Global conservation properties of the method have been investigated. Current analytical methods show that these relatively simple observation handles need to be augmented with additional mathematics similar to Akkerman et al. [2]. Further in depth review of the numerical behaviour of the method such as convergence proofs and error estimates together with a correct relation between the boundary and interior will reveal potential improvements on the analytical frame work.

Stabilization When this is achieved an appropriate stabilization scheme needs to be implemented to reduce instabilities occurring at high advection. For FEM Brooks and Hughes [9] showed that stability can be enforced on a local level with methods without affecting the physics too much. Methods such as SUPG locally stabilize the residual and energy descriptions for these methods are readily available.

Wave maker A wave maker boundary condition together with a dissipation boundary condition at the beach completes the numerical towing tank. The mesh motion now has to be extended to all directions. The dissipation at the beach ensures that the waves decay accordingly. Different implementations of these boundary conditions are showcased in [7][17] and [39].

Validation These results can then be validated and compared to empirical results. The potential flow equation should provide an accurate description of waves up to breaking. Interesting would be if high phase accuracy can be achieved. In [7][17] and [39] this still proved to be a challenge.

Optimization A quality sufficient for implementation of an optimization scheme to design an improved wave-maker startup routine to reduce non-linear effects. In [27] a number of these methods are addressed. Particularly interesting is the adjoint method

A

Derivation of Ideal Free-Surface Ideal flow

A.1. Bernoulli equations

To derive the equations for potential flow we start at the Incompressible Navier-Stokes Equations [24]

$$\rho \frac{\partial \mathbf{u}}{\partial t} + \rho(\mathbf{u} \cdot \nabla) \mathbf{u} = -\nabla \mathbf{p} + \mu \nabla^2 \mathbf{u} + \rho \mathbf{g} \quad (\text{A.1})$$

$$\nabla \cdot \mathbf{u} = 0 \quad (\text{A.2})$$

For fluid problems, certain characteristics can be defined by identifying some key physical parameters. These can be, for instance, length, density, viscosity or gravity. We can non-dimensionalize the Navier Stokes equations with these physical parameters. Here, define a characteristic density $\bar{\rho}$, length L and mean stream velocity U . Resulting in the non-dimensionalized Navier Stokes Equations. The characteristic timescale τ is a function of velocity and space.

$$\frac{\rho U}{\tau} \frac{\partial \mathbf{u}}{\partial t} + \frac{\rho U^2}{L} (\mathbf{u} \cdot \nabla) \mathbf{u} = -\frac{\pi}{L} \nabla \mathbf{p} + \frac{\rho U}{L^2} \mu \nabla^2 \mathbf{u} + \rho \mathbf{g} \quad (\text{A.3})$$

$$\nabla \cdot \mathbf{u} = 0 \quad (\text{A.4})$$

For the inertial regime we select $\pi = \rho U^2$. If we then divide the Navier Stokes Equations by $\rho U^2 / L$ we get the non-dimensional Navier Stokes Equations.

$$St \frac{\partial \mathbf{u}}{\partial t} + (\mathbf{u} \cdot \nabla) \mathbf{u} = -\nabla \mathbf{p} + \frac{1}{Re} \nabla^2 \mathbf{u} + \frac{1}{Fr^2} \mathbf{g} \quad (\text{A.5})$$

$$\nabla \cdot \mathbf{u} = 0 \quad (\text{A.6})$$

$$St = \frac{L}{U\tau} \quad \text{Strouhal number} \quad (\text{A.7})$$

$$Re = \frac{\rho UL}{\mu} \quad \text{Reynolds number} \quad (\text{A.8})$$

$$Fr = \frac{U}{\sqrt{gL}} \quad \text{Froude number} \quad (\text{A.9})$$

$$(\text{A.10})$$

For large Reynolds numbers, the viscous terms cancel and from that we obtain the Euler equations. Now if we also assume irrotationality, we can say that the velocity field derives from a potential.

$$\nabla \times \mathbf{u} = 0 \quad \text{irrotationality} \quad (\text{A.11})$$

$$\nabla \phi = \mathbf{u} \quad \text{velocity derives from a potential} \quad (\text{A.12})$$

we obtain

$$(\mathbf{u} \cdot \nabla) \mathbf{u} = \mathbf{u} \times \nabla \times \mathbf{u} + \nabla \frac{1}{2} (\|\mathbf{u}\|^2) \quad (\text{A.13})$$

Substitution in the reduced momentum equations and incompressibility statement.

$$\rho \frac{\partial \mathbf{u}}{\partial t} + \frac{1}{2} \rho \|\mathbf{u}\|^2 + \rho \mathbf{g} + \nabla p = 0 \quad (\text{A.14})$$

$$\nabla \left(\rho \frac{\partial \phi}{\partial t} + \frac{1}{2} \rho \|\phi\|^2 + p \right) + \rho \mathbf{g} = 0 \quad (\text{A.15})$$

$$\rho \frac{\partial \phi}{\partial t} + \frac{1}{2} \rho \|\nabla \phi\|^2 + p + \rho g z = C(t) \quad \text{Momentum} \quad (\text{A.16})$$

$$\nabla^2 \phi = 0 \quad \text{Mass conservation} \quad (\text{A.17})$$

A.2. Boundary conditions

For the case of the free-surface we define an additional physical boundary conditions apart from the momentum conditions which have to be met. Additionally a geometric or kinematic boundary condition has to be defined to preserve the interface.

$$p - p_a = \gamma \left(\frac{1}{R_1} + \frac{1}{R_2} \right) \quad \text{Normal stress boundary condition} \quad (\text{A.18})$$

With γ , being the kinematic viscosity, R_1 and R_2 are the principle radii of curvature and p_a is the atmospheric pressure. An ideal fluid can not exert any surface tension at a surface. Therefore at the free surface we have $p = p_a$. Consequently, the momentum equation at the free surface becomes

$$\frac{\partial \phi}{\partial t} + \frac{1}{2} \|\nabla \phi\|^2 + g\eta = 0 \quad (\text{A.19})$$

Next we define an equation for the free-surface.

$$H = \eta - z = 0 \quad (\text{A.20})$$

For the free surface to remain intact the following has to hold which gives rise to the kinematic boundary condition.

$$\frac{DH}{Dt} = \frac{\partial H}{\partial t} + \mathbf{u} \cdot \nabla H = 0 \quad (\text{A.21})$$

$$\frac{\partial \eta}{\partial t} + \nabla \phi \cdot \begin{bmatrix} \nabla \eta \\ -1 \end{bmatrix} = 0 \quad (\text{A.22})$$

B

Mathematical expressions

B.1. Reynold's Transport Theorem & Gauss' Divergence Theorem

$$\frac{d}{dt} \int_{\Omega(t)} q d\Omega \stackrel{RTT}{=} \int_{\Omega(t)} \frac{\partial q}{\partial t} + \nabla \cdot (q\mathbf{u}) d\Omega, \quad \int_{\Omega(t)} \nabla \cdot q d\Omega \stackrel{Gdt}{=} \int_{\Gamma(t)} q \cdot \mathbf{n} d\Gamma \quad (\text{B.1})$$

$$\Rightarrow \frac{d}{dt} \int_{\Omega(t)} q d\Omega = \int_{\Omega(t)} \frac{\partial q}{\partial t} d\Omega + \int_{\Gamma(t)} q\mathbf{u} \cdot \mathbf{n} d\Gamma \quad (\text{B.2})$$

B.2. Definition of kinetic and potential energy

$$E_{kin} \equiv \frac{1}{2} m \|\mathbf{u}\|^2 \quad (\text{B.3})$$

$$E_{pot} \equiv \int_0^\eta g z dz \quad (\text{B.4})$$

B.3. Green's identities

$$- \int_{\Omega} w \nabla^2 \psi d\Omega = \int_{\Omega} \nabla w \cdot \nabla \psi d\Omega - \int_{\Gamma} w (\nabla \psi \cdot \mathbf{n}) d\Gamma \quad (\text{B.5})$$

B.4. Boundary integral mapping

In this section we arrive at an expression for the boundary integrals

$$(w, \gamma \eta_t)_{\Gamma_{fs}(t)} = \int_{\Gamma_{fs}(t)} w \gamma \eta_t d\Gamma \quad (\text{B.6})$$

$$\int_{\Gamma_{fs}(t)} \gamma v \left(\frac{d\psi}{dt} + \frac{1}{2} \nabla \psi \cdot \nabla \psi + g \eta \right) d\Gamma \quad (\text{B.7})$$

In terms of the still water level Γ_0 . For now we assume no wave maker to be present. Remind us

$$\nabla \psi \cdot \mathbf{n} = \mathbf{u} \cdot \mathbf{n} = \gamma \eta_t \quad (\text{B.8})$$

From calculus we know that the surface integral of a function $f(x, y, z)$ over an domain \mathcal{S} can be expressed as

$$\int_{\Gamma} f(x, y, z) d\Gamma = \int_S f(x, y, g(x, y)) \sqrt{1 + (g_1(x, y))^2 + (g_2(x, y))^2} dA \quad (\text{B.9})$$

$$z = g(x, y) \quad (\text{B.10})$$

The free surface η is given to be

$$z = \eta(\mathbf{x}, t) \quad (\text{B.11})$$

For a transformation of the integrals from the moving free-surface the γ term drops out which corresponds to the cosine of the angle with the z axis.

$$\mathbf{n}_z = \cos\theta = \mathbf{n} \cdot \mathbf{e}_3 = \gamma \quad (\text{B.12})$$

As such we get

$$(w, \gamma \eta_t)_{\Gamma_{fs}(t)} = \int_{\Gamma_{fs}(t)} w \gamma \eta_t d\Gamma = \int_{\Gamma_0} w \eta_t dS \quad (\text{B.13})$$

$$\int_{\Gamma_{fs}(t)} \gamma v \left(\frac{d\psi}{dt} + \frac{1}{2} \nabla \psi \cdot \nabla \psi + g\eta \right) d\Gamma = \int_{\Gamma_0} v \left(\frac{d\psi}{dt} + \frac{1}{2} \nabla \psi \cdot \nabla \psi + g\eta \right) dS \quad (\text{B.14})$$

This makes sense as effectively a "larger" differential area is projected onto a smaller one whilst the integral remains the same.

B.5. Bilinear form

$$B(u + v, w) = B(u, w) + B(v, w) \quad (\text{B.15})$$

$$B(u, v + w) = B(u, v) + B(u, w) \quad (\text{B.16})$$

B.6. Luke's Principle

$$J = \int_{t_0}^{t_1} \int_{x_0}^{x_1} \mathcal{L} dx dt$$

Here we take the variation of the pressure

$$\mathcal{L} = \int_0^{h(x,t)} (p - p_0) d\Omega = - \int_0^{h(x,t)} \left(\frac{1}{2} \phi_x^2 + \frac{1}{2} \phi_y^2 + \phi_{,t} + g(y - H_0) \right) dy$$

If we vary J accordingly with respect to h and ϕ at the boundaries, Luke derives the following:

$$\delta J = \int_{t_0}^{t_1} \int_{x_0}^{x_1} \delta \mathcal{L} dx dt = 0$$

The delta is moved inside of the integral, due to the boundary values.

$$\delta \mathcal{L} = \int_0^{h(x,t)+\delta h} \left(\frac{1}{2} \|\nabla(\phi + \delta\phi)\|^2 + (\phi + \delta\phi)_{,t} + g(y - H_0) \right) dy - \int_0^{h(x,t)} \left(\frac{1}{2} \|\nabla\phi\|^2 + \phi_{,t} + g(y - H_0) \right) dy$$

The first term rewrites

$$\begin{aligned} & \int_0^{h(x,t)+\delta h} \left(\frac{1}{2} \|\nabla(\phi + \delta\phi)\|^2 + (\phi + \delta\phi)_{,t} + g(y - H_0) \right) dy \\ &= \int_0^{h(x,t)} \left(\frac{1}{2} \|\nabla(\phi + \delta\phi)\|^2 + (\phi + \delta\phi)_{,t} + g(y - H_0) \right) dy + \left[\frac{1}{2} \|\nabla(\phi + \delta\phi)\|^2 + (\phi + \delta\phi)_{,t} + g(y - H_0) \right]_{y=h} \delta h \end{aligned}$$

Neglecting higher order terms $\mathcal{O}(\delta^2)$

$$\begin{aligned} & \int_0^{h(x,t)+\delta h} \left(\frac{1}{2} \|\nabla(\phi + \delta\phi)\|^2 + (\phi + \delta\phi)_{,t} + g(y - H_0) \right) dy \\ &= \int_0^{h(x,t)} \left(\frac{1}{2} (\nabla\phi \cdot \nabla\phi + 2\nabla\phi \cdot \nabla(\delta\phi) + \nabla(\delta\phi) \cdot \nabla(\delta\phi)) + (\phi + \delta\phi)_{,t} + g(y - H_0) \right) dy + \left[\frac{1}{2} \|\nabla\phi\|^2 + \phi_{,t} + g(y - H_0) \right]_{y=h} \delta h \end{aligned}$$

Again, neglecting higher order terms $\mathcal{O}(\delta^2)$

$$\begin{aligned} \delta \mathcal{L} &= \left[\frac{1}{2} \|\nabla\phi\|^2 + \phi_{,t} + g(y - H_0) \right]_{y=h} + \int_0^{h(x,t)} \nabla\phi \cdot \nabla(\delta\phi) + \delta\phi_{,t} dy \\ \Rightarrow \delta J &= \int_{t_0}^{t_1} \int_{x_0}^{x_1} \left\{ \left[\frac{1}{2} \|\nabla\phi\|^2 + \phi_{,t} + g(y - H_0) \right]_{y=h} \delta h + \int_0^{h(x,t)} \nabla\phi \cdot \nabla(\delta\phi) + \delta\phi_{,t} dy \right\} dx dt = 0 \quad (\text{B.17}) \end{aligned}$$

C

FEM example: advection diffusion

This example serves as a short introduction into FEM by means of the advection-diffusion equation where given $u \in \mathbb{R}$, $\epsilon \in \mathbb{R}$ and $f : [0, L] \rightarrow \mathbb{R}$ we need to find $\phi \in \mathbb{R}$ such that

$$u\phi_{,1} + \epsilon\phi_{,11} = f$$

The weak form of the problem reads that given $u \in \mathbb{R}$, $\epsilon \in \mathbb{R}$ and $f : [0, L] \rightarrow \mathbb{R}$ we need to find $\phi \in \mathbb{R}$ such that $\forall w \in \mathcal{W}$,

$$\int_{\Omega} -w_{,1}u\phi + w_{,1}\epsilon\phi_{,1} dx = \int_{\Omega} wf dx. \quad (C.1)$$

We will approximate the solution to Equation (C.1) using the Bubnov-Galerkin method and C^0 piecewise-linear finite element spaces $V_{1,h}^0$. With the above choice of finite elements, the trial and test function spaces are chosen as below,

$$\mathcal{S}_h := \left\{ f \in V_{1,h}^0 : f(0) = 0, f(L) = 1 \right\}, \quad \mathcal{W}_h := \left\{ f \in V_{1,h}^0 : f(0) = 0, f(L) = 0 \right\}$$

The weak form of the problem is

$$\int_{\Omega} w_{,1}u\phi + w_{,1}\epsilon\phi_{,1} - wf dx = 0$$

Next, the infinite dimension spaces can be replaced by the finite dimension spaces.

$$\phi_h = \sum_j B_j \phi_j, \quad w_h = \sum_i B_i w_i$$

Substituting for w and ϕ and using bilinearity gives

$$\sum_{i=1}^{n-1} w_i \sum_{j=0}^n \int_0^L (-B_{i,1}uB_j\phi_j + B_{i,1}\epsilon B_{j,1}\phi_j - B_i f) dx = 0$$

To solve for an element i we look at a schematic representation of the elements here it can be seen that when $|i - j| > 1$ the integral is equal to zero. As such, we can rewrite this into

$$\sum_{j=i-1}^{i+1} \int_{x_{i-1}}^{x_{i+1}} (-B_{i,1}uB_j\phi_j + B_{i,1}\epsilon B_{j,1}\phi_j - B_i f) dx = 0 \quad (C.2)$$

Let consider the four non-zero cases of Equation (C.2) depicted in table 11 Substitution of the basis functions in Equation (C.2) gives the following equation

$$\begin{aligned} & \int_{x_{i-1}}^{x_i} -\frac{u}{h} \left(1 - \frac{1}{h}(x - x_{i-1})\right) \phi_{i-1} - \frac{1}{h^2} \epsilon \phi_{i-1} dx + \int_{x_{i-1}}^{x_i} -\frac{u}{h} \frac{1}{h} (x - x_{i-1}) \phi_i - \frac{1}{h^2} \epsilon \phi_i dx \\ & + \int_{x_i}^{x_{i+1}} \frac{u}{h} \left(1 - \frac{1}{h}(x - x_i)\right) \phi_i + \frac{1}{h^2} \epsilon \phi_i dx + \int_{x_i}^{x_{i+1}} \frac{u}{h} \frac{1}{h} (x - x_i) \phi_{i+1} - \frac{1}{h^2} \epsilon \phi_{i+1} dx \\ & + \int_{x_{i-1}}^{x_{i+1}} B_i f dx = 0 \end{aligned}$$

$x \in [x_{i-1}, x_i), \quad j = i - 1$	$B_{i-1} = 1 - \frac{1}{h}(x - x_{i-1})$ $B_{i-1,1} = -\frac{1}{h}$
$x \in [x_{i-1}, x_i), \quad j = i$	$B_i = \frac{1}{h}(x - x_{i-1})$ $B_{i,1} = \frac{1}{h}$
$x \in [x_i, x_{i+1}), \quad j = i$	$B_i = 1 - \frac{1}{h}(x - x_i)$ $B_{i,1} = -\frac{1}{h}$
$x \in [x_i, x_{i+1}), \quad j = i + 1$	$B_{i+1} = \frac{1}{h}(x - x_i)$ $B_{i+1,1} = \frac{1}{h}$

Table 11: Piecewise basis function

These are solved and combined resulting in

$$h \left[u \frac{\phi_{j+1} - \phi_{j-1}}{2h} - \epsilon \frac{\phi_{j+1} - 2\phi_j + \phi_{j-1}}{h^2} - \frac{1}{h} \int_{x_{j-1}}^{x_{j+1}} B_i f dx \right] = 0$$

For every element i . Results are plotted in Figure 33. For Peclet number higher than one the solution shows to be unstable. The Peclet number is defined by

$$Pe_h = \frac{|u|h}{\epsilon} \tag{C.3}$$

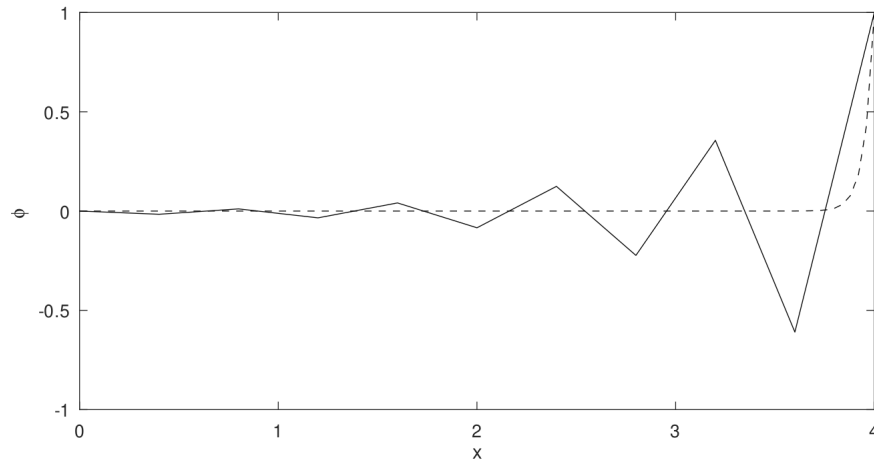


Figure 33: Galerkin approximation of the Advection Diffusion equation. The dashed line indicates the exact solution. $Pe_h = 8$

D

Wave maker derivations

Pitching wave maker boundary condition For the wave maker a boundary condition in parametric form could be the following

$$\begin{aligned}\theta_{wm} &= \theta_{wm}^{max} \sin(\omega_{wm} t) \\ \dot{\theta}_{wm} &= \theta_{wm}^{max} \omega_{wm} \cos(\omega_{wm} t) \\ \mathbf{u} \cdot \mathbf{n} &= s \dot{\theta}_{wm}\end{aligned}$$

Here $s \in [0, L_{wm}]$ is a parameter denoting the position along the wave maker and a is a control parameter for the wave maker frequency.

$$\mathbf{u} \cdot \mathbf{n} = s \omega_{wm} \theta_{wm}^{max} \cos(at) \quad (D.1)$$

Energy evolution with wavemaker BC

After integration by parts, the Neumann boundary condition for the wavemaker can be substituted in. This is a natural boundary condition.

$$-(w, \Delta \psi)_{\Omega(t)} = (\nabla w, \nabla \psi)_{\Omega(t)} - (w, \nabla \psi \cdot \mathbf{n})_{\Gamma_{fs}(t)} = (w, \nabla \psi \cdot \mathbf{n})_{\Gamma_{wm}(t)}$$

Doing the same as previously we find that with the included forcing term the total energy evolution is a function of the wave-maker energy. From here onwards we will no longer address the wave maker boundary condition as this is beyond the scope of this thesis.

$$\frac{d}{dt} \left(\frac{1}{2} (\nabla \psi, \nabla \psi)_{\Omega(t)} + \int_{\Omega(t)} g z d\Omega \right) = \frac{1}{4} \omega_{wm}^2 L_{wm}^2 (\theta_{wm}^{max})^2 \cos^2(\omega_{wm} t) \quad (D.2)$$

E

Code Snippets

E.1. C++

Listing E.1: Mesh file for a 2D unit square

```
1 MFM NURBS mesh v1.0
2
3 # 2D square mesh
4
5 dimension
6 2
7
8 elements
9 1
10 1 3 0 1 3 2
11 boundary
12 4
13 1 1 0 1
14 2 1 1 3
15 3 1 3 2
16 4 1 2 0
17
18 edges
19 4
20 0 0 1
21 1 0 2
22 0 2 3
23 1 1 3
24
25 vertices
26 4
27
28 patches
29
30 knotvectors
31 2
32 1 2 0 0 1 1
33 1 2 0 0 1 1
34
35 dimension
36 2
37
38 controlpoints
39 0 0 1
40 1 0 1
41 0 1 1
42 1 1 1
```

Listing E.2: Periodicity file

1 | 1

2 | 4 2

E.2. C

Listing E.3: local . bcs file for version A

```
1 | bnd    form    phi eta
2 | 1      0      0  1
3 | 2      0      0  0
4 | 3      1      0  0
5 | 4      0      0  0\n
```

Listing E.4: local . bcs file for version B

```
1 | bnd    form    phi eta
2 | 1      0      0  1
3 | 2      0      0  0
4 | 3      1      0  1
5 | 4      0      0  0\n
```

F

Running DelFI

DelFI runs through the Command Line Interface (CLI). When changes are made that need to be compiled into binaries, DelFI has to be recompiled. Other changes which only dependent on ASCII input such as mesh files, need no recompilation of DelFI. Recompilation is done in the build folder with the command `make`. To speed up the process, compilation can be done in parallel with `make -j 6`, e.g. for 6 processes. A typical run command is given by

```
mpirun -np 1 ../../delfi -m square.mesh -physics LinearisedWave -r 2 -tf 10.0
-dt 0.01 -eo -vis 0.01 -ni 10 -s 32 -o 2 -lt 1e-6 -nt 1e-3 -bcp 0 -d99 0 -b local.bcs
-p local.per | tee log;
```

The first argument is to run DelFI in parallel using MPI. The flag `-np`, followed by an integer indicates the number of processes/threads which we would like to use. Next the location of executable file of DelFI is given. Consequently, the user specifies MPI to run the `delfi` executable with 1 process. Expressions starting with a dash are called flags. These flags are followed by an input for DelFI. By running `delfi -help`, definitions of these flags can be found.

The boundary conditions are specified in a `.bcs` file (Appendix E.3 E.4). The first column corresponds to the boundary identifiers specified in the `.mesh` file. The second column corresponds to a marker which can be used to evaluate a residual boundary formulation, such as the free-surface description, only on the indicated boundary.

Bibliography

- [1] I. Akkerman and M. F.P. ten Eikelder. Toward free-surface flow simulations with correct energy evolution: An isogeometric level-set approach with monolithic time-integration. *Computers & Fluids*, 181:77–89, mar 2019. ISSN 0045-7930. doi: 10.1016/J.COMPFLUID.2019.01.015.
- [2] I. Akkerman, J. H.A. A Meijer, and Marco F.P. P Ten Eikelder. Isogeometric analysis of linear free-surface potential flow. *Ocean Engineering*, 201, apr 2020. ISSN 00298018. doi: 10.1016/j.oceaneng.2020.107114.
- [3] Ido Akkerman. Delft Finite Element and Iso Geometric Analysis (DelFI). 2021. URL <https://gitlab.tudelft.nl/idoakkerman/delfi.git>.
- [4] Robert Anderson, Julian Andrej, Andrew Barker, Jamie Bramwell, Jean Sylvain Camier, Jakub Cerveny, Veselin Dobrev, Yohann Dudouit, Aaron Fisher, Tzanio Kolev, Will Pazner, Mark Stowell, Vladimir Tomov, Ido Akkerman, Johann Dahm, David Medina, and Stefano Zampini. MFEM: A modular finite element methods library. *Computers and Mathematics with Applications*, 81:42–74, 2021. ISSN 08981221. doi: 10.1016/j.camwa.2020.06.009. URL <https://doi.org/10.1016/j.camwa.2020.06.009>.
- [5] V. I. Arnold. *Mathematical methods of classical mechanics*. Springer-Verlag,, New York :, 1989. ISBN 0387968903.
- [6] Marc Bonnet. *Boundary integral equation methods for solids and fluids*. J. Wiley,, Chichester :, 1995. ISBN 0471971847.
- [7] Freekjan Brink, Ferenc Izsák, and J. J.W. van der Vegt. Hamiltonian Finite Element Discretization for Nonlinear Free Surface Water Waves. *Journal of Scientific Computing*, 73(1):366–394, 2017. ISSN 08857474. doi: 10.1007/s10915-017-0416-9.
- [8] L. J. F. Broer. On the hamiltonian theory of surface waves. *Applied Scientific Research*, 29(1):430–446, 1974. ISSN 0003-6994. doi: 10.1007/BF00384164. URL <http://link.springer.com/10.1007/BF00384164>.
- [9] Alexander N Brooks and Thomas J R Hughes. STREAMLINE UPWIND/PETROV-GALERKIN FORMULATIONS FOR CONVECTION DOMINATED FLOWS WITH PARTICULAR EMPHASIS ON THE INCOMPRESSIBLE NAVIER-STOKES EQUATIONS. *COMPUTER METHODS IN APPLIED MECHANICS AND ENGINEERING*, 32:199–259, 1982.
- [10] T.H.J. Bunnik, E. van Daalen, G.K. Kapsenberg, Y. Shin, R.H.M. Huijsmans, G. Deng, G. Delhommeau, M. Kashiwagi, and B. Beck. A comparative study on the state-of-the-art prediction tools for seakeeping, 2010. URL <http://resolver.tudelft.nl/uuid:28b1781c-3ed2-4f9b-bf40-fa4d10b28dc1>.
- [11] E. Campana, F. Lalli, and U. Bulgarelli. A boundary element method for a non-linear free surface problem. *International Journal for Numerical Methods in Fluids*, 9(10):1195–1206, 1989. ISSN 10970363. doi: 10.1002/fld.1650091003.
- [12] Hank Childs, Eric Brugger, Brad Whitlock, Jeremy Meredith, Sean Ahern, David Pugmire, Kathleen Bigas, Mark C Miller, Cyrus Harrison, Gunther H Weber, Hari Krishnan, Thomas Fogal, Allen Sander-son, Christoph Garth, E Wes Bethel, David Camp, Oliver Rubel, Marc Durant, Jean M Favre, and Paul Navratil. VisIt: An End-User Tool For Visualizing and Analyzing Very Large Data, 2012. URL <https://visit.llnl.gov>.
- [13] R. Coifman. The fast multipole method for the wave equation: a pedestrian prescription. *IEEE antennas & propagation magazine*, 35(3):7–12, 1993. ISSN 1045-9243.
- [14] Kristian Dysthe, Harald E Krogstad, and Peter M Uller. Oceanic Rogue Waves Freak wave: term used interchangeably with rogue wave. *Annu. Rev. Fluid Mech*, 40:287–310, 2008. doi: 10.1146/annurev.fluid.40.111406.102203. URL www.annualreviews.org.

- [15] Sylvain Nintcheu Fata. Fast Galerkin BEM for 3D-potential theory. 42:417–429, 2008. doi: 10.1007/s00466-008-0251-9.
- [16] John Fenton. John Fenton's homepage - last updated 19 April 2021. URL <https://www.johndfenton.com/>.
- [17] Floriane Marie Pauline Gidel. Variational water-wave models and pyramidal freak waves. (June), 2018. URL <http://theses.whiterose.ac.uk/21730/>.
- [18] L. J. Gray, J. M. Glaeser, and T. Kaplan. Direct Evaluation of Hypersingular Galerkin Surface Integrals. <http://dx.doi.org/10.1137/S1064827502405999>, 25(5):1534–1556, jul 2006. doi: 10.1137/S1064827502405999.
- [19] Takanori. Hino, Frederick (Professor of engineering) Stern, Lars. Larsson, Michel. Visonneau, Nobuyuki. Hirata, and Jin. T A T T Kim. Numerical ship hydrodynamics : an assessment of the Tokyo 2015 workshop, 2021. URL <https://doi.org/10.1007/978-3-030-47572-7><https://ezproxy.lau.edu.lb:2443/login?url=https://doi.org/10.1007/978-3-030-47572-7>.
- [20] Leo H. Holthuijsen. *Waves in Oceanic and Coastal Waters - Knowel*, volume 9780521860. Cambridge University Press, jan 2007. ISBN 9780511618536. doi: 10.1017/CBO9780511618536. URL https://app-knovel-com.tudelft.idm.oclc.org/web/toc.v/cid:kpWOCW0002/viewerType:toc//root_{_}slug:waves-in-oceanic?kpromoter=marc.
- [21] T. J.R. Hughes, J. A. Cottrell, and Y. Bazilevs. Isogeometric analysis: CAD, finite elements, NURBS, exact geometry and mesh refinement. *Computer Methods in Applied Mechanics and Engineering*, 194(39-41): 4135–4195, oct 2005. ISSN 00457825. doi: 10.1016/j.cma.2004.10.008.
- [22] Thomas J. R. Hughes. *The Finite Element Method: Linear Static and Dynamic Finite Element Analysis*, 1987. ISSN 1467-8667.
- [23] J.W. W. Kim and K.J. J. Bai. A finite element method for two-dimensional water-wave problems. *International Journal for Numerical Methods in Fluids*, 30(1):105–122, may 1999. ISSN 0271-2091. doi: 10.1002/(SICI)1097-0363(19990515)30:1<105::AID-FLD822>3.0.CO;2-F. URL [https://onlinelibrary.wiley.com/doi/10.1002/\(SICI\)1097-0363\(19990515\)30:1{ }3C105::AID-FLD822{ }3E3.O.CO;2-F](https://onlinelibrary.wiley.com/doi/10.1002/(SICI)1097-0363(19990515)30:1{ }3C105::AID-FLD822{ }3E3.O.CO;2-F).
- [24] Pijush K. Kundu. *Fluid mechanics*. Academic Press :, London :, 2016. ISBN 9780124059351.
- [25] Michel Visonneau Lars Larsson, Frederick Stern. *Numerical ship hydrodynamics.*, volume 94 of *Lecture Notes in Applied and Computational Mechanics*. Springer International Publishing, Cham, 2010. ISBN 0917936116. doi: 10.1007/978-94-007-7189-5. URL <http://link.springer.com/10.1007/978-3-030-47572-7>.
- [26] Lars Larsson and Hoyte C. Raven. *Experimental Resistance Prediction and Flow Measurement. In: The Principles of Naval Architecture Series - Ship Resistance and Flow*. 2010. URL https://app-knovel-com.tudelft.idm.oclc.org/web/toc.v/cid:kpPNASSRF2/viewerType:toc//root_{_}slug:principles-of-naval?kpromoter=marc.
- [27] J. M. Lewis, S. Lakshmivarahan, and Sudarshan Kumar Dhall. *Dynamic data assimilation : a least squares approach*. Cambridge University Press,, Cambridge :, 2006. ISBN 9781461941507.
- [28] J. C. Luke. A variational principle for a fluid with a free surface. *Journal of Fluid Mechanics*, 27(2):395–397, feb 1967. ISSN 14697645. doi: 10.1017/S0022112067000412. URL <https://doi.org/10.1017/S0022112067000412>https://www.cambridge.org/core/product/identifier/S0022112067000412/type/journal_{_}article.
- [29] Person and Gloria Dickie. Tsunami models underestimated Shockwave from Tonga eruption, jan 2022. URL <https://www.reuters.com/world/asia-pacific/tsunami-models-underestimated-shockwave-tonga-eruption-2022-01-28/>.

- [30] Les. Piegl and Wayne. T A T T Tiller. The NURBS Book, 1997. URL <http://public.ebookcentral.proquest.com/choice/publicfullrecord.aspx?p=3092619><https://archive.org/details/nurbsbook00piegh><https://doi.org/10.1007/978-3-642-59223-2><http://link.springer.com/10.1007/978-3-642-59223-2><https://openlibrary.org/books/OL1008193>.
- [31] Athanasios G. Polimeridis and Traianos V. Yioultsis. On the Direct Evaluation of Weakly Singular Integrals in Galerkin Mixed Potential Integral Equation Formulations. *IEEE Transactions on Antennas and Propagation TA - TT -*, 56(9):3011–3019, 2008. ISSN 0018-926X. doi: 10.1109/TAP.2008.928782LK-<https://tudelft.on.worldcat.org/oclc/4798720147>.
- [32] Hoyte C. Raven. *A Solution Method for the Nonlinear Ship Wave Resistance Problem*. TU Delft, 1996. ISBN 9075757034. URL <http://resolver.tudelft.nl/uuid:dc8bed91-6b88-4366-84ea-d54ef5af3da9>.
- [33] Jean Jacques Risler. Computer aided geometric design. *Handbook of Numerical Analysis*, 5:715–818, 1997. ISSN 15708659. doi: 10.1016/S1570-8659(97)80006-3.
- [34] Paul D Sclavounos. Stability analysis of free-surface panel methods for the wave resistance problem. 31(0):149–152, 1988. URL <http://resolver.tudelft.nl/uuid:40caa361-0bfc-4c2d-9753-69ef76ba68b8>.
- [35] James Serrin. Mathematical Principles of Classical Fluid Mechanics. pages 125–263, 1959. doi: 10.1007/978-3-642-45914-6_2. URL https://link.springer.com/chapter/10.1007/978-3-642-45914-6_{_}2.
- [36] G.G. Stokes. On the theory of oscillatory waves. *Mathematical and Physical Papers*, vi, 1847.
- [37] Jos van Kan, Guus Segal, and Vermolen Fred. Numerical methods in scientific computing. 2005.
- [38] Frans. van Walree. Computational Methods for Hydrofoil Craft in Steady and Unsteady Flow. page 374, 1999. ISSN 1464-3405. URL <https://repository.tudelft.nl/islandora/object/uuid:eb3e6fd9-05c8-4b1d-8836-b996e4985190?collection=research>.
- [39] Jaap-Harm Westhuis. The numerical simulation of nonlinear waves in a hydrodynamic model test basin. *Thesis*, page 262, 2001.
- [40] Jonathan Whiteley. Mathematical Engineering Finite Element Methods A Practical Guide. Technical report. URL <http://www.springer.com/series/8445>.
- [41] G . B . Whitham. Variational Methods and Applications to Water Waves, A Discussion on Nonlinear Theory of Wave Propagation. *Proceedings of the Royal Society of London . Series A , Mathematical and Physical Sciences*, 299(1456):6–25, 1966.
- [42] Jon Wilkening. Traveling-Standing Water Waves. *Fluids 2021, Vol. 6, Page 187*, 6(5):187, may 2021. ISSN 2311-5521. doi: 10.3390/FLUIDS6050187. URL <https://www.mdpi.com/2311-5521/6/5/187/html><https://www.mdpi.com/2311-5521/6/5/187>.
- [43] G. X. Wu and R. Eatock Taylor. Finite element analysis of two-dimensional non-linear transient water waves. *Applied Ocean Research*, 16(6):363–372, jan 1994. ISSN 01411187. doi: 10.1016/0141-1187(94)00029-8.
- [44] G. Y. Yu and S. C. Fan. Symmetric BEM formulations for 2-D steady-state and transit potential problems. *Computers and Structures*, 81(1):27–37, jan 2003. ISSN 00457949. doi: 10.1016/S0045-7949(02)00347-4.